Final Report
Absolute age dating of fracture filling minerals
to investigate the stability of the geosphere in southern Ontario (R613.3)
presented to Canadian Nuclear Safety Commission
March 2017

J. Spalding, D.A. Schneider
Department of Earth & Environmental Sciences, University of Ottawa, Canada

Included: Summary of Activities, Analytical Methods, 10 Figures, 2 Tables, 6 Appendices (A-F)

Understanding the structural geology, paleoseismology, and structural history of the bedrock of southern Ontario is an important strategy of the Canadian Nuclear Safety Commission (CNSC) and their partners, since they are, in part, responsible for the safe storage of Canada's nuclear waste in deep geologic repositories (DGR). Of particular relevance is the tectonic stability of the geosphere in the region of the storage facilities. Over long geologic time, the host rock will be an important barrier to contaminant migration from repository waste. Determining the geologic stability of the region involves not only mapping the geometry and orientation of faults and fractures, but also understanding their age of (re)activation and strain behavior (seismic or aseismic). The objective through this research is to develop a project to map the brittle tectonic structures, assess their deformation mechanism, and provide numerical (radiometric) age constraints on faulting across strategic sites across southern Ontario.

Field Location: Prince Edward County, Ontario

Research projects assessing the stability of the geosphere have been pursued in Bruce Peninsula, Ontario, by Cruden (2011) and Davis (2013), among others. It is logical to expand the local perspective beyond Bruce Peninsula to gain a broader understanding on the stability of the geosphere in Southern Ontario. Doing so seemed beneficial, such that it allowed us to use preliminary results from Bruce Peninsula as framework during interpretation of our results.

Prince Edward County was chosen as a field area for three reasons: 1) the Cobourg Formation that is proposed to host DGR at a depth of ~680 meters below the surface at Bruce Peninsula is the stratigraphic equivalent of the rock units exposed at the surface of Prince Edward County. Surficial exposure of these rock formations provides a unique opportunity to study how brittle deformation manifests itself in these rock units beyond the confinement of core logs and could potentially be useful for scientists working on the DGR. 2) Prince Edward County is located at the intersection of the Salmon River-Picton fault system with the Hamilton Presqu'île lineament. These faults are seismically active, therefore providing an ideal location to map brittle deformation. 3) There is abundant bedrock exposure along the northern shore of Lake Ontario. Field work in southern Ontario can be problematic due to the relatively flat topography, and very little outcrop exposure, this problem was side-stepped by choosing Prince Edward County as a field location, which hosts exposure of the fault systems mentioned above.

Summary of activities and data presentation

Field work was conducted during the summers of 2015 and 2016. A total of ~20 days were spent conducting field work. We identified 32 stations recording brittle deformation, and collected 38 samples from 15 of the stations. The geographic distribution of station locations is presented in **Figure 1**. The UTM coordinates of each station, a complete sample list corresponding to each station, and summary of analyses done on each sample is reported in **Table 1**. Structural measurements from each station are presented on Rose diagrams in **Figure 2**, with the corresponding structural data available in Appendix A. Field photos are available in Appendix B with sub-folders corresponding to each station, and a document containing photo descriptions. Uncovered polished thin sections were successfully prepared for 25 of our samples. Photomicrographs in plane light, cross-polarized light, and cathodoluminescence (CL) are available in Appendix C with sub-folders corresponding to each station and a document containing the photomicrograph descriptions. The full Analytical Methods are available at the end of this document.

Trace element geochemistry was conducted during the spring of 2016 on 31 samples of mineral separates via LA-ICP-MS at the University of Ottawa. Data was normalized to chondritic composition and plotted on spider diagrams organized by their respective station, presented in **Figure 3**. During the winter of 2016-2017, we conducted in-situ analyses (100 μm thick sections) for trace element geochemistry on five veins. We complemented point analysis with a series of rastered traverses across the width of calcite veins. Results from the in-situ trace element geochemical analysis are presented in **Figures 4-8**. All geochemical results are available in Appendix D (reported at σ_1) from mineral separates and in-situ analyses.

Stable isotope analysis of $\delta^{13}C$ and $\delta^{18}O$ was accomplished during the fall of 2016 at the G.G. Hatch Laboratories at the University of Ottawa on 36 samples. Results from stable isotope analysis are presented in **Figure 9**, with their absolute values available in Appendix E.

During the summer of 2016, we spent five weeks dating calcite via (U-Th)/He geochronology at University of Paris-South (Orsay) under the direction of Dr. Cécile Gautheron. A total of 16 samples were analyzed during this time, with multiple replicates on each sample. Because of abundant fluid inclusions, the analyses contained unsupported and variable amounts of He, yielding very old and dispersed dates. These values are meaningless, and have been excluded from the report. The fluid inclusions, however, open an opportunity to further explore the source of the fluids via measured $^3He/^4He$ ratios. Eight samples are being analyzed for $^3He/^4He$ concentrations, of which we have received preliminary results from two of our samples and are awaiting results from the other six samples in the coming weeks. $^3He/^4He$ values are presented in **Table 2**, and samples that we are expecting results are noted in **Table 1**.

In August and November 2016, seven samples were selected for radiometric dating via U-Pb at the University of Toronto with the assistance of Dr. Don Davis. Concordia diagrams are presented in **Figure 10**, and results from the analysis are available in Appendix F. Furthermore, the results and data of the seven samples dated via U-Pb are highlighted by unique symbols throughout this report.

Field work

The purpose of field work was two-fold: 1) map and collect structural data on brittle structures preserved in the bedrock, and 2) sample fracture-filling minerals for geochemical analysis and dating. While conducting field work, we attempted to locate outcrops over a broad geographic distribution, both proximal and distal to fault traces and identify structures that record

evidence of reactivation, (e.g. slicken-slide fabrics, and offset) as well as their mechanism of deformation. Through first-order principals of relative chronology (e.g. terminating joint relationships) and by inferring the modern stress field, the youngest joint population observed has a broad E-W orientation. We strategically focussed on sampling calcite veins from dilated joints with a broad E-W orientation to constrain the most recent deformation event.

Station locations are labelled with Roman numerals. Their geographic distribution is represented in **Figure 1**, with their UTM coordinates listed in **Table 1**. Sub-vertical structural measurements, including joints, fractures and veins from each station are represented on Rose diagrams in **Figure 2**. Outcrops that did not preserve brittle deformation were assigned numerals during field work, but have been excluded from the report, hence the discontinuous numerals ranging from I to XLIV. Given the proximity at the University of Ottawa to our field area, we found it practical to do field work in increments. This allowed us time to strategically plan each field trip, and target new areas, and reflect on stations that require more attention. Samples collected from the field season of 2015 are labelled with the prefix "PEC-15," and samples collected during the field season of 2016 are labelled with the prefix "PEC-16." See Analytical Methods for additional details.

Field season 2015

Five field excursions took place during the late summer/fall of 2015: August 9th to 11th 2015, September 3rd to 5th, and November 12th to 15th 2015 and two day-trips exclusively visiting the Intalcamenti Quarry (Station I) on September 21st and October 19th 2015. Prior to beginning field work, we created a plan based on 1) coordinates documented in published literature reporting brittle structures and 2) preliminary geological maps of the Paleozoic geology of southern Ontario from the Ontario Geological Survey to locate fault traces. We found literature from the1960's to 1990's (e.g. Cuddy, 1969; McFall and Allam, 1992; McFall, 1993) reporting brittle structures such as pop-up structures and faulting, however when following the coordinates, the locations were often covered in vegetation, or inaccessible due to steep cliffs. Upon this realization, we altered our field plan. By reconnoitering the peninsula, we quickly observed that rock exposure was best preserved along river banks, road cuts, and the shore along Lake Ontario and focussed our attention on these locations. During our field work in 2015 we identified 20 stations with prominent structural features ranging from station I to XXIX. From the 20 outcrops identified, we collected a total of 29 calcite veins from 13 of the stations. Two calcite veins (PEC-15-14 and PEC-15-31B) had multiple crystal morphologies along a continuous vein. The calcite in these veins were separated (in the lab) and independently analyzed to yield a total of 31 samples.

Our interest in visiting the Intalcamenti Quarry (station I) was based on publications reporting calcite mineralization and faulting along the excavation walls. During our visit, we exclusively visited the southern excavation. We observed joint sets trending 085°/77° and 300°/86° (photo I-554). The excavation preferentially fractures along calcite veins, exposing ~60 meters in height of fractured surface with calcite mineralization on the quarry wall surface. We also observed slicken-slide fabric and intense fracture zones approximately 15 m in width. Minor offset on a normal fault plane oriented at 300°/80° (photo I-648). In the quarry, there is a Jurassic ultramafic dyke intruding the Paleozoic strata that is cross cut by calcite fracture splays (Barnett et al, 1984). We collected a sample of the ultramafic dyke containing one vein with two distinct crystal morphologies that were manually separated while sampling: an elongated slicken-slide fabric (PEC-15-14I), and a more prominent fibrous/tabular crystal habit (PEC-15-14II) intact within the host rock.

Calcite veins exceeding a width of 3 mm were found almost exclusively along the southern shore of Lake Ontario in joints oriented WSW-ESE, however hairline veins are also present at these locations (photo IV-712). Eight stations were located along the southern shore of Lake Ontario, six of which we could sample calcite veins. At station X, a dilated joint oriented at 271° hosts a calcite vein that is locally brecciated, and vug-filled (photo X-751). We separated these two crystal morphologies: PEC-15-31BI consists of the vein itself, and sample PEC-15-31BIII is euhedral crystals that fills "vugs" along the vein.

Station VI, XVIII, XIX and XX are beach outcrops along irregular shaped eastern arms in the north-east arms of the peninsula. Station VI preserves the same joint density and orientation as outcrops on the southern shore (photo VI-184), however stations XVIII, XIX and XX located ~15 km to the north, preserve no NW oriented joints, and a lower joint density.

The mainland of the peninsula (excluding quarries) consist of five stations. Four of these stations (VII, VIII, XIII and XVIII) expose ~30 meters of outcrop that have preferentially eroded along joint surfaces that locally preserve calcite mineralization on joint surfaces (photo XVIII-497). At station VII we locally observed a sub-horizontal slicken-slide fabric along a calcite vein with euhedral overgrowth of calcite crystals, suggesting the joint has dilated to accommodate a second generation of mineralization. We were unable to sample the slicken-slide fabric (photo VII-688), however we sampled euhedral overgrowth crystals from two veins: PEC-15-2A and PEC-15-27 (photo VII-682).

Station XIII is located ~15 km north of Prince Edward County along the trace of the Salmon River faults within the Gull River Formation. This station visited based on literature reporting neo-tectonic fault reactivation (Mitchell, 2007). We observed, pencil cleavage oriented 10°-072° (photo XIII-301), and minor vein offset. Calcite veins did not exceed hairline width, however we collected samples PEC-15-6 and PEC-15-7 (photo XIII-299).

Field season 2016

Two field excursions took place during the summer of 2016: June 28th to 29th, and July 25th to 26th. We focused on locating new stations preserving densely spaced joints along the shore line of Lake Ontario, as well as visiting new quarries. We used satellite imagery via GoogleEarth to design our field plan. During the 2016 field season, we located three new stations along the shore lines of Lake Ontario, six limestone quarries, and revisited stations requiring additional measurements.

Three new stations located on the shoreline of Lake Ontario: station XXXVII, XXXVIII and XXXIX. Stations XXXVII and XXXIX are located to the east of the Picton Fault trace and preserve a more prominent NW-SE oriented joint population and a secondary population with a broad E-W orientation. Notably, station XXXVII is located to the west of Picton Fault trace and preserves a NE-SW oriented joint population. Among the new stations located along the shorelines of Lake Ontario, calcite veins were only observed at station XXXIX, where sample PEC-16-5 was collected (photo XXXIX-2071). Three locations that we had anticipated on visiting were inaccessible due to private properties or poor road conditions (station XLI, XLII and XLII). Prominent joints are observable along the shoreline of Lake Ontario, and the trends are measurable via GoogleEarth. The orientation of measurements taken via GoogleEarth are in agreement to the orientations of structures measured in the field. These stations are included in the Rose plots of **Figure 2** of this report.

In the six limestone quarries visited, the excavation preferentially fractures along joint surfaces, with the most prominent joints oriented broadly E-W. Stations XXXII and XXXV

preserve secondary joint populations oriented S-SW (photo XXXV-2048). Unlike the Intalcamenti Quarry visited in 2015 (station I) the excavation walls preserve little or no calcite mineralization. Due to security regulations, station XXXII was the only quarry where we could collect samples: sample PEC-16-4A, PEC-16-4B, and PEC-16-4C. Sample PEC-16-4C is quartz vein with euhedral crystals up to 0.8 cm in width (photo XXXII-2032).

We also revisited sites that required additional measurements and material. At station XXVI we collected sample PEC-16-1 and PEC-16-2, and at station VII we collected sample PEC-16-3.

Petrography

Calcite veins were often eroded along the vein-wallrock interface. Thin-section preparation was problematic for exposed calcite veins preserving less than 1 mm of mineralization. Micro-structures revealed through petrography of calcite veins, as well as intra-crystalline deformation in calcite crystals provides information on crystallization processes, evidence for episodic fluid flow, and deformation processes.

Crystallization processes

Calcite veins that are ~1 mm in width are characterized by large equant sized crystals in the center of the vein with a reduction of crystal size at the vein-wall-rock interface (photo PEC-15-8_1). The relationship of these crystal morphologies is characteristic of syntaxial-bitaxial vein growth, where initial nucleation initiates on both sides of the host rock, forming small crystals. Subsequent crystallization at a slower growth rate allows large, equant crystals to grow at center of the vein. Crystal growth is initiated from both sides of the vein at similar rates leads to "competition growth," where the internal crystals of the vein are equidimensional (Fisher and Brantley, 1992; Bons and Jessell 1997). During syntaxial-biaxial growth a median line is generally preserved in the center indicating the last stage of crystal growth. This line was only observed in one sample (photo PEC-15-6_1).

In sample PEC-15-2C, we observe a reduction of crystal size on only one side of the vein-wallrock interface with elongated, tabular shaped crystals filling the vein. The asymmetry of the crystals suggest that nucleation originated from one side of the vein. Uniaxial growth results in there being no "growth-competition," allowing crystal growth to continue, perpendicular to the wall-rock and fill the entire width of the vein with tabular crystals (photo PEC-15-2C_1).

Episodic fluid-flow

Our observations in thin veins (~1 mm in width) are characterized by equant shaped calcite crystals with a reduction of crystal size at the vein-wallrock interface (discussed above). By inferring this characteristic in larger calcite veins (>3 mm), a pattern in crystal morphology can be used to identify multiple generations of fluid flow through vein reactivation (e.g. photo PEC-15-31A_1). If a vein is continuously reactivated, a median line should develop where fluid flow occurs This is a rare scenario, and often vein reactivation occurs randomly throughout the vein, cutting through pre-existing crystals and not preserving a median line. None of our poly-phase calcite veins preserve a median line. The internal structure of poly-phase veins appears to be massive, with vein reactivation (small crystals) occurring closer to the edges of the veins. Veins can be reactivated along the vein-wallrock interface without permanently opening the vein (photo PEC-31BI). The asymmetry and irregularity of poly-phase veins makes it difficult to resolve the relative

timing of fluid flow of the sub-veins corresponding to different pulses of fluid. Vein genesis can however be resolved from cross-cutting relationships of the veins (photo PEC-16-1_1).

We took CL images of poly-phase veins to get a qualitative perspective on the chemical variation from different fluid pulses within a single vein. Most secondary veins appear to all have similar composition under cathodoluminescence (e.g. PEC-15-5B_1), whereas some showed distinct compositions, varying in luminescence (PEC-16-1_2). Luminescence through CL is controlled primarily by the presence of Mn, and lack of Fe, therefore a lack of chemical variation along different veins cannot be ruled out based solely on uniform crystal luminescence under CL.

Deformation

Macroscopically, calcite veins preserve evidence of shearing with a ~350 μm offset of fossil fragments (photo PEC-15-32B_1), and locally calcite veins accommodate compression through pressure solution at grain boundaries (photo PEC-15-5A_5). Deformation accommodated by calcite veins is best understood by studying the intra-crystalline micro-structures within calcite crystals. Twinning is the dominant crystal-plastic low temperatures deformation mechanism temperatures in calcite crystals. Type I are twins that appear as thin black lines (<10 μm), and are associated to deformation below 170°C. Calcite twins that develop at higher temperatures develop color fringes with measurable widths, (lamellar twinning), corresponding to temperatures of ~200°C (Turner, 1953). The thickness of calcite twins is inversely correlated with twin density (twin/mm): at lower temperature, closely spaced type I twins dominate calcite crystals, while at higher temperatures dispersed thick lamellar twins dominate calcite crystals (Ferrill, 1991). Lamellar twins are indicative of higher strain as they tend to develop along crystal boundaries (photo PEC-15-31C_3). In some veins, entire crystals are twinned, which can be indicative of continuous deformation, allowing lamellar twins to migrate laterally into un-twinned portions of the crystal, eventually sweeping the entire crystal (PEC-16-4C_1) (Rutter 1995). Aside from twinning, undulous extinction is also indicative of low temperature deformation in calcite (photo PEC-15-31A_4). Exceeding temperatures of ~250-300°C, calcite begins to undergo recovery through dynamic recrystallization. Lamellar twins become tapered, and develop lensoid shapes (photo PEC-15-25DII_3). Eventually, recrystallization will overprint primary structures, and erase pre-existing twins within the crystal. Evidence of recrystallization is preserved through sub-grain growth development, where sub-grains possess different extinction angles (photo PEC-15-25DI_1). Complete recrystallization is also observed through “jig-saw-like” grain boundaries (photo PEC-25-C_1; Groshong, 1988; Burkhard, 1993).

In some calcite veins, different populations of calcite crystals can be identified based on their twinning densities in different crystals. For example, in sample PEC-15-31C we identified crystals with exclusively type I twins, with an average twin thickness of ~8 μm, and a density of 11 twins/mm, whereas other crystals with lamellar twins have an average thickness of ~65 μm width and a density of 3 twins/mm (photo PEC-15-31C_2). Similarly, in sample PEC-15-31A a calcite crystal with extensive lamellar twins cross-cuts a recrystallized calcite crystal with no twins (photo PEC-15-31A_3). We locally observe lamellar twins that are kinked, broken and offset, suggesting that the calcite experience low temperature post-twinning brittle deformation (photo PEC-15-25DII_2).

Trace element geochemistry

During the winter of 2015-2016 trace element geochemistry was done via LA-ICP-MS at the University of Ottawa on 31 mineral separates. Up to six analytical points were taken on each sample, with at least one crystal selected for two-point analysis per sample. The main purpose of conducting trace element geochemistry was to identify samples with the highest ^{238}U content as these samples would be the best candidates for U-Pb and (U-Th)/He geochronology. During the analysis, we also measured: Mg, Si, Mn, Fe, Sr, Y, Ba, Th and REE's (**Figure 3**).

Sample PEC-15-30 has the highest ^{238}U content of with average of ~50 ppb. Point analysis from different grains vary from 0-510 ppb. Two point analyses within the same crystal measure the same value (320 ppb and 318 ppb), suggesting the distribution of U varies from crystal to crystal within the calcite vein. Furthermore, the point analysis recording 510 ppb of ^{238}U also exhibited elevated ^{29}Si content (6557 ppm), suggesting that the single point analysis could be representative of an inclusion. Samples PEC-15-31A, PEC-15-8, PEC-15-2C and PEC-15-2A record relatively high ^{238}U values, with an average from 57-90 ppb. Their ^{238}U values vary on two orders of magnitude, however from the 31 samples these are the only four samples that consistently measured ^{238}U values on every point analysis. Based on our preliminary geochemical work, these five samples were prioritized for geochronology.

Our samples are relatively depleted in Y, with values <10 ppm. Notably, samples collected in the west of our field area, proximal to the Hamilton-Presqu'ile lineament, are enriched in Y: at station XVI, sample PEC-15-8 has Y values of ~205 ppm. The station to the east (station XI) has Y values of 28 ppm and 11 ppm from samples PEC-15-5A and PEC-15-5B, respectably.

Other trace elements such as Mn, Mg, and Sr vary within samples from crystal to crystal. For example, Mg in sample PEC-15-9 varies from 255-1722 ppm, its Mn content varies from 561-1006 ppm and its Sr content varies from 30-92 ppm. This variability is also observed in crystals with multiple point analysis, for example two point analyses from a single crystal in sample PEC-15-8 has Mg values of 916 ppm and 472 ppm, Mn values of 11058 and 5794 ppm and Sr values of 64 ppm and 192 ppm. These observations suggest that trace elements, like U, are not distributed homogenously across calcite veins, or within crystals. The average values from our geochemical analysis are 1500 ppm of Mg, 1180 ppm of Mn, and 165 ppm of Sr. Sr values are more consistent within samples, and can be used to group samples into three main categories: samples a depleted Sr population (<120 ppm), consisting of 14 samples, a "normal" Sr population (120-190 ppm), consisting of 11 samples and a population that is enriched in Sr (>190 ppm), consisting of six samples. Despite the defined three Sr groups, no correlation existed between these groups and other elemental variables or observations.

REE values were normalized to chondritic composition, and we created spider-plots organized by their respective stations in **Figure 3**. In general, the REE profiles follow a negative slope from LREE to HREE with a negative Eu anomaly. The relative abundance of REE's and fractionation varies from sample to sample, for example at station VII sample PEC-15-27 and PEC-15-2A exhibit similar profiles, however profiles from sample PEC-15-2A are confined to vary under one order of magnitude, whereas sample PEC-15-27 has elevated concentrations over three orders of magnitude. REE fractionation can be attributed to variations of crystal chemistries across calcite veins, as observed in Mg, Mn and Sr concentrations. Geochemical analysis on mineral separates provides no spatial resolution on the location of calcite crystals within the vein. To understand how trace elements are distributed across poly-phased veins, a second-round of trace-element geochemistry on 100 μm thick sections was conducted. We selected traverses across calcite veins where measurements were rastered across the width of the vein. By aligning photomicrographs of the ablated traverses with the signal acquired, we could identify chemical

variations that correlate to crystal boundaries, fluid inclusions and crystal zonation (**Figure 4-8**). To quantify these chemical variations, we also measured a series of point analysis adjacent to the traverse where we targeted crystals with different morphologies, as well as distinguish between the composition of the cores and rims of zoned crystals. For example, in sample PEC-15-8 crystals with reduced grain size at the vein-wall rock interface are attributed with an enrichment of Sr, and equant crystals in the center of the vein are zoned in ^{238}U. In a larger composite veins (e.g. samples PEC-15-5A and PEC-15-31A), different vein segments of polyphase veins vary in Sr, ^{238}U and REE's abundances, and elevated concentrations are often aligned with opaque material in plane light microscopy residing at recrystallized grain boundaries.

$\delta^{13}C$ and $\delta^{18}O$ stable isotopes

All calcite veins were analyzed except for two samples: one that did not provide sufficient material (PEC-15-14II), and the quartz vein (PEC-16-4C) yielding a total of 36 samples. $\delta^{13}C$ values are normalized to V-PDB with values ranging between -0.92‰ and 6.2‰. $\delta^{18}O$ values are normalized to V-SMOW with values ranging between 19.52‰ and 24.85‰. As previously mentioned, the host rock of all calcite veins is Middle Ordovician limestone. **Figure 9** shows the results of the stable isotope analyses, with a box defining the composition of Middle Ordovician limestone. Half of the samples plot within this box, and most others plot with elevated $\delta^{18}O$ values that can be explained by warmer water temperatures during fluid flow and crystallization. Four samples possess enriched $\delta^{13}C$ values (>5‰): samples PEC-15-2A, PEC-15-25A, PEC-15-27 and PEC-15-31BIII. Samples PEC-15-2A and PEC-15-27 were collected from veins with exposed calcite mineralization and euhedral calcite crystals. Also, sample PEC-15-31B is a calcite vein that was separated based on different crystal morphologies: Sample PEC-15-31BIII are large crystals picked from (late) vug-filled segments of the calcite vein and has a $\delta^{13}C$ value of 6.3‰, whereas the dominant part of the vein (sample PEC-15-31BI) is relatively depleted in $\delta^{13}C$ at 0.64‰. Three samples are relatively depleted in $\delta^{18}O$ (<20‰): samples PEC-15-5A, PEC-15-5B and PEC-15-13. In addition, two samples (PEC-16-4A and PEC-16-4B) collected from station XXXII (the Foster Rock Limestone Quarry) have anomalous values that are relatively enriched in $\delta^{18}O$ (>24‰) as well as $\delta^{13}C$ values (>3‰) compared to the composition of Middle Ordovician limestone. Note that these samples were proximal to the quartz vein (sample PEC-15-4C), and that these samples were not analyzed for trace elements being they were collected during the field season of 2016. All our stable isotope values are similar in compositions to Middle Ordovician limestone, therefore the fluid from which the calcite veins crystallized is interpreted to originate from connate fluids released from pores in the limestone during deformation. Slight variations in the stable isotope signatures can be attributed to the evolution of the fluid, where heavier isotopes reside in the fluid during crystallization, and buffering from the fluid interacting with the host rock.

U-Pb and (U-Th)/He geochronology

We spent one month at the University of Paris-South (Orsay) to conduct (U-Th)/He dating on calcite separates that yielded high U (or Th) concentrations. Despite abundant helium concentrations, (U-Th)/He dating was unsuccessful yielding highly dispersed dates likely from excess He derived from the fluid inclusions, commonly along fractures. However, preliminary $^{3}He/^{4}He$ analyses indicate a primitive, deep fluid signature (R/Ra: 0.5-2.7) for the fluid inclusions. Seven samples were strategically selected for LA-ICP-MS U-Pb geochronology at the University

of Toronto to obtain crystallization ages of calcite veins. We attempted to date calcite veins from each population defined from our stable isotope diagram (**Figure 9**). The four samples that consistently yielded ^{238}U above detection limits during trace element geochemical analysis provided the most reliable model ages (**Figure 10**; PEC-15-2A, PEC-15-2C, PEC-15-8, PEC-15-31A). Between 9 and 17 point analyses were used from each sample, providing model ages ranging between 81.4 ± 8.3 (MSWD: 2.6) and 110.7 ± 6.8 (MSWD: 0.53). Sample PEC-15-30 was chosen due to its high ^{238}U content, despite some point analysis with unmeasurable ^{238}U values. This sample generated a meaningless model age of -164 ± 270 (MSDW: 6). From the three samples that are relatively depleted in $\delta^{18}O$ (<20‰), sample PEC-15-5A had the highest ^{238}U content (~16 ppb), and was selected for U-Pb geochronology. We analyzed 10 spots for this sample, that were strongly discordant therefore no model age was calculated. Sample PEC-15-25A, with ^{238}U values of ~6 ppb, yielded a five point analysis with concordant measurements and a model age of 120 ± 63 (MSWD: 1.16). Since all veins are sampled from joints with the same E-W to NE-SW trend, we regressed all the calcite dates together, yielding an age of 101 ± 6 Ma (MSWD: 2.3).

Preliminary interpretations

Multiple periods of fault reactivation have been recognized in southern Ontario in response to an evolving stress field. Work by Rimando et al. (2005) identified three periods of fault reactivation (D_1, D_2 and D_3), each associated with different tectonic events where the applied stress field (σ_1) has undergone a counter-clockwise rotation. D_1 is associated with the closing of Iapetus with σ_1 oriented NW-SE, D_2 associated with the opening of the Atlantic in the Mesozoic with σ_1 oriented WNW-ESE, D_3 is associated with the stress field since the Cretaceous generated from ridge push during expansion of the Atlantic Ocean with σ_1 oriented WSW-ENE (Rimando et al., 2005). From our field work we observe two prominent joint populations: NW-SE and a broad E-W orientation, where E-W oriented joints often terminated upon intersecting NW-SE oriented joints. Based on terminating joint relationships, and by inferring the findings of Rimando et al. (2005), we interpret NW-SE oriented joints to have formed are a result of D_1, and broadly oriented E-W structures are a result of D_2 and potential reactivation during D_3. Dilated joints later served as pathways to accommodate fluid flow, crystallizing the calcite veins sampled in this study.

Intra-crystalline micro-structures such as extensive lamellar twinning, undulous extinction, pressure solution at grain boundaries and dynamic recrystallization indicate that calcite veins have undergone deformation temperatures of ~250°C. However, twins that are kinked and broken, suggest calcite has under gone post-twinning brittle deformation, and that the deformation history of the calcite veins was cyclical and complex. Poly-phase veins are also characteristic of cyclical deformation, where deformation increases pore-fluid pressure initiating fluid flow, followed by crystallization when pore-fluid pressure drops. Microstructural analysis and polyphase-vein growth suggest that deformation was synchronous and potentially outlasted fluid flow. The source of the calcite veins is believed to be connate fluids derived from the host Middle Ordovician bedrock, based on $\delta^{13}C$ and $\delta^{18}O$ values resembling the composition of Middle Ordovician bulk limestone compositions and REE profiles plotting similar compositions to the upper continental crust. Preliminary $^{3}He/^{4}He$ analyses record a primitive, deep fluid signature component (R/Ra: 0.5-2.7) for the fluid inclusions trapped within the calcite, suggesting that fluid sources from mixed reservoirs.

By coupling our microstructural observations, geochemical analysis and U-Pb ages, we suggest that Prince Edward County was affected by a regional brittle deformation event at c. 100

Ma which released connate fluids from pore-space, that migrated along pre-existing E-W oriented joints. Our results and preliminary interpretation in Prince Edward County can be compared to similar studies conducted at Bruce Peninsula, Ontario. Cruden (2011) report two major joint populations in the Devonian rocks: a prominent NNW oriented set and a secondary set oriented ENE, hosting calcite mineralization. These veins within the Devonian strata were dated Davis (2013), yielding ages of 100 Ma and a subordinate event around 50 Ma. Rock cores of the Ordovician units at depth remain relatively unfractured, hosting thin calcite veins. These veins were also dated by Davis (2013), recording ages of 445 ± 42 Ma, approaching the age of diagenesis of the host rock.

Thus, rocks at the surface in Bruce Peninsula and Prince Edward County have undergone comparative deformation histories: preserving similar joint densities with slightly different orientations that hosts extensive calcite mineralization with U-Pb crystallization ages of c. 100 Ma. The Algonquin Arch forms a structural high that divides Bruce Peninsula (Michigan Basin) from Prince Edward County (Appalachian Basin), and it is possible that the ages from these two locations do not record the same event despite recording similar dates. However, if the 100 Ma ages in Bruce Peninsula and Prince Edward County record the same event, that would suggest that regional deformation is confined to the surficial rocks, given that Ordovician rocks in Bruce Peninsula at a depth of ~680 m below the surface are unfractured with U-Pb ages resembling diagenesis the timing of diagenesis.

Prince Edward County is located ~200 km to the west of the c. 140-120 Ma alkaline igneous rocks which mark the surface trace of the Great Meteor Hotspot. It is unlikely that our c. 100 Ma ages record this event, being that the great meteor hotspot would have been off the coast of Maine by 100 Ma. The period of 110-90 Ma has been identified as a global-scale plate reorganization that involved tectonic and magmatic events, and is preserved as a kink in the surface expression of the Great Meteor Hotspot track (Eaton and Frederiksen, 2007). We believe that our calcite veins were formed from fluid flow generated by this global scale plate reorganization event.

Final work

We are still conducting additional $^{3}He/^{4}He$ analyses, and are in the process of compiling our structural measurements, trace element data and $\delta^{13}C$ and $\delta^{18}O$ values into ARC GIS. The purpose of this is to build a geographic distribution of our data, that may not seem apparent (e.g. higher trace elements concentrations proximal to fault traces). Spalding is writing up and will be defending her thesis this summer.

Dissemination of results

Throughout the course of this research project, preliminary results have been presented at ASERC-2016 in Ottawa, EGU-2016 in Vienna, GAC-MAC-2016 in Whitehorse and we have submitted abstracts to GAC-MAC-2017 in Kingston. Spalding also gave a seminar at the University of Paris-South in June 2016. In the coming months, we will continue to interpret the implication of our results, and write a manuscript that will be submitted to an international peer reviewed journal.

Spalding, J., Schneider, D.A., Gautheron, C., Sarda, P., Davis, D., Petts, D.C., 2017. Geochronology and geochemistry of calcite-filled fractures, southern Ontario: insight into

Cretaceous plate reorganization? Geological Association of Canada Abstracts (Kingston, Canada).
Davis, D., Thibodeau, A., Spalding, J., Sutcliffe, C., Smith, P., Schneider, D., Adams, J., Zajacz, Z., Cruden, A., Parmenter, A., 2017. Secondary calcite as a useful U-Pb geochronometer: An example from the Paleozoic sedimentary sequence in southern Ontario. Geological Association of Canada Abstracts (Kingston, Canada).
Spalding, J., Schneider, D.A., Brown, J., 2016. Long-term stability at the edge of the Canadian Shield: Insights from calcite-filled fractures inherited from basement structures, southern Ontario, Canada. Geological Association of Canada Abstracts (Whitehorse, Canada).
Spalding, J., Schneider, D.A., 2016. Microstructural analysis of calcite-filled fractures inherited from basement Structures, southern Ontario, Canada: Long term instability of the craton? University of Paris-South (Orsay) Seminar Series (Paris, France).
Spalding, J., Schneider, D.A., 2016. Microstructural analysis of calcite-filled fractures inherited from basement structures, southern Ontario, Canada: long term instability of the craton? European Geoscience Union, EGU2016-10896 (Vienna, Austria).
Spalding, J., Schneider, D.A., 2016. Microstructural analysis of calcite-filled fractures inherited from basement Structures, southern Ontario, Canada: Long term instability of the craton? Advances in Earth Sciences Research Conference (Ottawa, Canada).

Analytical methods

Field work and structural measurements

We used maps published by the Ontario Geological Survey to locate major faults and outcrops in Prince Edward County (P2375, Carson, 1980; P2413 Carson, 1981; P2412, Carson, 1981, P2497, Carson, 1982). Fault traces are rarely exposed, and the exact locations are often supported by magnetic lineaments (2587, Ontario Geological Survey, 1991). During our first field excursions, we attempted to find fault exposure by following published coordinates. Cuddy (1969) reports exposure of the Picton Fault ~1 km north of Point Petre in a broad valley trending 020°, that is filled with glacio-fluvial sediments, however no exact coordinates were provided. We were unable to locate this valley, although the shore line at Point Petre (Station IV) preserved pervasive joint sets hosting calcite mineralization. Along the eastern arm of the peninsula, McFall (1993) reports minor E-W and NW oriented faults that host calcite veins, as well as pop-up structures. The UTM coordinates of the pop-up structures brought us to station V. This location was forested, we observed dilated joints that were filled with vegetation, however no pop-up structures were observed. The UTM coordinates where McFall reports minor faults were often along steep cliffs and the outcrop was only accessible by boat, except for station XXVIII where we observed minor faults. McFall (1993) also reports extensive calcite mineralization in the Essroc Intalcamenti Quarry (Station I). Mitchell (2007) reports horizontal offset of drill holes in outcrop adjacent to the trace of the salmon river fault. Since 2007, this road has been widened and most of these features have disappeared (Station XIII). All outcrop exposures within the peninsula (in forested areas and roadside outcrops) were generally covered in vegetation. Most published maps are out of date for locating suitable outcrops.

Published studies from Prince Edward County reports that brittle deformation is best preserved along shorelines of Lake Ontario. Prominent joint pattern in shallow waters of Lake Ontario can be observed from GoogleEarth. After our second field trip in 2015, our field plan was

based on stations located via GoogleEarth preserving extensive joint patterns. GoogleEarth was also used to locate six limestone quarries that were visited in 2016.

Structural measurements were taken with a Brunton compass, using the right-hand rule. The measurements were projected on Rose plots for each station using a Python script. The number of bins size varies on the number of structural measurements taken. At stations where less than eight measurements were taken, the number of bins is equal to the number of measurements. At stations where more than eight structural measurements were taken, the number of bins follows the following formula:

$$\text{bins} = 5\sqrt{n + 10},$$

where n = number of bins. From trial and error, we found this formula to best represent our structural data.

Sample characterization and imaging

Polished thin sections (30 μm thick) were prepared for 25 samples. Analysis was conducted via Olympus BX41 binocular polarizing microscopes and images were acquired using Image-Pro software package. Larger structures requiring a magnification less than 5X (i.e. photos of entire veins) were analyzed with a WILD Makroscope, attached to a Canon camera. Both microscopes are equipped for both transmitted and reflected light capabilities. In addition, cathodoluminescence (CL) microscopy was performed on representative thin sections. The CL microscopy was done on a CITL Mk5 Optical Microscope Stage. General operating conditions were a beam energy (accelerating voltage) of 78-27 kv, beam current of 460-600 milliamperes, and operating vacuum of 0.03-0.05 torr. Scanning electron microscopy (SEM) images were taken with a JEOL 6610LV Scanning Electron Microscope using secondary electron imaging in a high vacuum with a 1.7 kV beam at the University of Ottawa.

Trace element geochemistry via LA-ICP-MS

Mineral separates

Calcite crystals were manually separated from the host rock vein. The crystal size varied in each sample from <200 μm to ~3 mm. From samples with smaller crystals, we targeted the largest crystals with defined crystal habit. Crystals larger that 1.5 mm were crushed and sieved, and we targeted crystals without obvious fluid inclusions or discoloration. Five to eleven mineral separates were selected from each sample, and mounted onto four epoxy mounts that were organized by crystal size. Every crystal was analyzed, and one crystal from each sample was analyzed twice.

Trace element geochemistry was done at the University of Ottawa using the Photon Machines Analyte Excite 193 nm excimer laser coupled with an Agilent 7700x ICP-MS. The laser beam diameter for was 90 μm with a repetition rate of 10 Hz and a fluence of 7 J/cm^2. Each point analysis consisted of 30 s of background measurement, 50 s of ablation followed by 30 s of flushing the system. Each analysis measured Mg, Si, Mn, Fe, Sr, Y, Ba, La, Ce, Pr, Nd, Sm, Eu, Gd, Tb, Dy, Ho, Er, Tm, Yb, Lu, ^{204}Pb, ^{207}Pb, ^{208}Pb, ^{232}Th and ^{238}U.

The analyses were calibrated to the internal standard NIST-612, which was analyzed after every five unknowns. MACS-3 was used as an external standard. Calcium values were measured adjacent to each point analysis using a using a JEOL JXA-8230 Superprobe at the University of Ottawa, which were input to *Glitter* software to convert our measurements from counts/second to ppm values. *Glitter* was also used to isolate an appropriate signal for each measurement. The instrumentation has a detection limit for each element. A limit of quantification is defined as three

times the detection limit. To avoid biases from instrumentation, all values below the limit of quantification been rejected and attributed a value of zero during data reduction.

In situ analysis

Trace element geochemistry was measured on 100 μm-thick sections from five samples. A series of traverses across the width of calcite veins were conducted using 90 μm beam size with a repetition rate of 15 Hz and a fluence of 7 J/cm^2. Traverses consist of one continuous measurement during the ablation of the traverse. The signal acquired from the traverse can be used to show relative variations and distribution of trace elements across calcite veins by aligning photomicrographs to the ablated traverse with the raw signal (**Figure 4-8**). The absolute values of the signal acquired are equivocal. To resolve this problem and calibrate the acquired signal, in-situ point analysis were done adjacent to the traverse profiles. The analytical conditions and data reduction for the in-situ point analysis are the same as the point analysis done on mineral separates, however Zr was measured and ^{204}Pb was not. The absolute values acquired from the point analysis were added to the traverse signal aligned to photomicrographs. The raw signal was vertically adjusted to fit point analysis that are representative of the composition along the ablated traverse, (i.e. within the same crystal).

δ^{13}C and δ^{18}O Stable Isotope analysis

Calcite was separated from the veins, crushed into a fine powder, and weighed into exetainers with 0.1 mL of H_3PO_4 (S.G. 1.91). The exetainers are capped and helium-flushed while horizontal. Reaction at 25°C for 24 hrs is followed by extraction in continuous flow. The measurements are performed on a Delta XP and a Gas Bench II, both from Thermo Finnigan. See Application Flash Report G31 from Thermo Finnigan for instrument details. Analytical precision (2 sigma) is ±0.1‰. Oxygen data was normalized using international standards NBS-18, NBS-19, and carbon data was normalized using international standards NBS-18, NBS-19, and LSVEC. δ^{13}C and δ^{18}O values were measured relative to V-PDB. δ^{18}O V-PDB values were converted to δ^{18}O V-SMOW values by using the following formula:

$$\delta^{18}\text{O V-SMOW} = 1.0309\ \delta^{18}\text{O V-PDB} + 30.92$$

U-Pb geochronology via LA-ICP-MS

U-Pb analysis was conducted on the same mineral separates analyzed during trace element geochemistry. Samples were ablated and analyzed using a New Wave UP-193 laser ablation system with a 193 nm beam coupled to an Agilent 7900 ICPMS at the University of Toronto. The laser beam diameter for calcite was in the range 100-150 microns, 10 Hz, with a fluence of about 5 J/cm^2. Frequency and beam size were reduced for the NIST612 glass standard and appropriate correction factors applied to calculate U concentrations of samples. Measurements were carried out on ^{206}Pb, ^{207}Pb and ^{238}U as well as ^{232}Th to test for detrital material or alteration. Spots were pre-ablated by rastering the beam over an area larger than the beam diameter to clean the surface. Following a 10 s period of baseline accumulation the laser sampling beam was turned on and data were collected for 25 s followed by a washout period.

Data reduction used VBA software written by D. Davis (University of Toronto). Data acquisition involves collecting hundreds of cycles of ^{207}Pb, ^{206}Pb and ^{238}U measurements as the beam penetrates deeper into the sample and displaying the ratios in a time-resolved profile. The traditional approach to data reduction is to define an acceptable window within the data profile and average the ratios. Calcite typically has low (<1 ppm) U concentrations and the most useful

samples for dating are those with very low initial common Pb concentrations so that a significant proportion of the Pb is radiogenic. Relatively young (<100 Ma) radiogenic samples will have much lower Pb concentrations than U. One problem with averaging ratios is that when the signal approaches baseline ratios become unstable since a near-zero measured value in the denominator will cause the apparent ratio to increase without limit so the average tends to skew toward higher values. One way to prevent this is to base the average ratio on the sum of total counts in the numerator and denominator peaks. A discussion of the statistical theory is given in (Ogliore et al., 2011). One limitation is that calculation of standard deviations cannot be based on the scatter of individual measurements as in the ratio average approach. A standard deviation for a ratio can only be calculated based on the root-mean-square of $1/\sqrt{N}$ where N is the number of counts in each measurement. This will be a minimum estimate of the true standard deviation. The total standard deviations (sigma) for concordia coordinates and their cross correlations (rho) are determined by increasing each input parameter (measured sample and standard ratios) by one sigma, calculating the results and then taking the root-mean-square values of the deviations of these results from the means to produce variances and covariance for the mean concordia coordinate values.

Another problem with data collected from calcite is that there are often numerous spikes, particularly on the Pb isotopes, due to the explosive nature of the ablation process. Therefore, some data sets may have to be heavily edited. In the ratio averaging approach, anomalously high or low $^{207}Pb/^{206}Pb$ and $^{206}Pb/^{238}U$ ratios can be edited out independently. In the peak summing approach, peaks rather than ratios are edited and the rejection of one peak requires removal of all other peaks in the cycle. In most cases anomalous spikes are much higher than surrounding signals so the choice of which ones to edit is obvious, but this is not always the case so there is the danger of over-editing, which could bias data. The current software version has an 'auto edit' feature that allows peaks to be edited out to a chosen multiple of a standard deviation ($1/\sqrt{N}$).

Time resolved profiles of ratios for zoned calcite often show variable $^{207}Pb/^{206}Pb$ and $^{206}Pb/^{238}U$ values, which may be due either to variable age or to variations in the ratio of U to initial common Pb. A feature of the new software is that it presents a time resolved profile of model ages. Where data are sufficiently precise, this allows resolution and averaging of specific age zones. This software appears to result in more consistent and statistically robust ages. Meaningful age information can be extracted even when Pb signals are only a few counts in each cycle. Reduced data are plotted and averaged using Isoplot (Ludwig 2003). Ages and error ellipses are given at 2 sigma unless otherwise noted.

References

Barnett R.L., Arima M., Blackwell J.D., Winder C.G., 1984. The Picton and Varty Lake ultramafic dikes: Jurassic magmatism in the St. Lawrence Platform near Belleville, Ontario. Canadian Journal of Earth Sciences, 1460-1472.

Bons P.D., Jessell M.W., 1997. Experimental simulation of the formation of the formation of fibrous veins by localized dissolution-precipitation creep. Mineral Magazine 61, 53-63

Burkhard, M., 1993. Calcite twins, their geometry, appearance and significance as stress–strain markers and indicators of tectonic regime: a review. Journal of Structural Geology 15, 351–368

Carson, D.M., 1980. Paleozoic geology of the Trenton-Concecon area, southern Ontario. Ontario Geological Survey, Preliminary Map P.2375

Carson, D.M., 1981. Paleozoic geology of the Tichborne-Sydenham area, southern Ontario. Ontario Geological Survey, Preliminary Map P.2413

Carson, D.M., 1981. Paleozoic geology of the Belleville-Wellington area, southern Ontario. Ontario Geological Survey, Preliminary Map P.2412.

Carson, D.M., 1982. Paleozoic geology of the Bath-Yorkshire area, southern Ontario. Ontario Geological Survey, Preliminary Map P.2497

Cruden, S., 2011. Outcrop fracture mapping. NWMO TR-2011-43

Cuddy, R.G., 1969. A preliminary study of the Picton Fault Zone, B.Sc. thesis, Queen's University, Kingston ON Canada, 154 pp

Davis, D., 2013. Application of U-Pb geochronology methods to the absolute age of determination of secondary calcite. NWMO TR-2013-21

Eaton D.W., Frederiksen A., 2007 Seismic evidence for convection-driven motion of the North American plate. Nature Letters volume 446

Ferrill, D.A., 1991. Calcite twin widths and intensities as metamorphic indicators in natural low-temperature deformation of limestone. Journal of Structural Geology 13, 667–675

Fisher D.M., Brantley S.L., 1992. Models of quartz overgrowth and vein formation: Deformation and episodic fluid flow in an ancient subduction zone. Journal of Geophysical Reasearch. 97, 20043–20061

Groshong, R.H. Jr, 1988. Low-temperature deformation mechanisms and their interpretation. Geological Society of America Bulletin 100, 1329–1360.

Ludwig, K.R., 2003. User's manual for Isoplot 3.00 a geochronological toolkit for Excel. Berkeley Geochronological Center Special Publication 4, 71 p.

McFall, G.H. 1993. Structural elements and neotectonics of Prince Edward County, southern Ontario, Géographie Physique et Quaternaire, 47: 303-312.

McFall, G.H., Allam, A., 1991. Neotectonic investigations in southern Ontario: Prince Edward county - Phase II. Research report for the Atomic Energy Control Board, Project No. 3.131.2

Mitchell, F., 2007. Structural analysis of brittle deformation features along Grenvillian shear zones in southeastern Ontario, Queen's University, Kingston ON Canada, 154 pp

Ogliore, R.C. Huss, G.R., Nagashima, K. 2011. Ratio estimation in SIMS analysis. Nuclear Instruments and Methods in Physics Research B 269: 1910–1918

Ontario Geological Survey, 1991. Total-field aeromagnetic of Ontario-southern sheet. Map 2587

Rimando, R.E., Benn, L., 2005. Evolution of faulting and paleo-stress field within the Ottawa graben, Canada. Journal of Geodynamics 39, 337–360

Rutter, E.H., 1976. The kinetics of rock deformation by pressure solution. Philosophical Transactions of the Royal Society of London A283, 203–219

Turner, F.J., 1953. Nature and dynamic interpretation of deformation lamellae in calcite of three marbles. American Journal of Science 251, 276–298

Table 1: Station locations, sample list and summary of geochemical analysis done on calcite veins collected from Prince-Edward-County, Ontario

Station	UTM Coordinates	Rock Formation	Comment	Joint measurements (n)	Sample number	Vein orientation	Vein thickness/ comment	Thin Section	Stable Isotope	Trace elements	U-Pb	$^3He/^4He^*$
I	328992.51W 4880483.13N	Veralum	Quarry: *ESSROC Italcamenti*	20	PEC-15-12B	085/86	Exposed	Y	Y	Y	-	-
					PEC-15-13	035/86	Exposed	-	Y	Y	-	Y
					PEC-15-14I	-	<1 mm; slicken-slide	Y	Y	Y	-	-
					PEC-15-14II		1 mm; fibrous/tabular		-	Y	-	-
II	328912.29W 4877573.52N	Lower Lindsay	Behind Picton Harbor	3	PEC-15-25A	065/74	1.5 mm	-	Y	Y	Y	N/A
					PEC-15-25B	052/78	1.3 mm	-	Y	Y	-	-
					PEC-15-25C	190/07	5 cm	Y	Y	Y	-	N/A
					PEC-15-25DI	-	3.3 mm	Y	Y	Y	-	-
					PEC-15-25DII	-	3 mm	Y	Y	Y	-	-
IV	327140.55W 4856320.58N	Upper Lindsay	Lake Ontario Shoreline: Point Petre	69	PEC-15-29	229	1.5 mm	Y	Y	Y	-	-
V	331722.60W 4860580.30N	Lower Lindsay	Forested area	3	-	-	-	-	-	-	-	-
VI	344898.80W 4865785.70N	Veralum	Peninsula shoreline	15	-	-	-	-	-	-	-	-
VII	335812.83W 4870075.04N	Lower Lindsay	Roadside outcrop: County Rd 16	40	PEC-15-2A	250/78	Exposed	Y	Y	Y	Y	N/A
					PEC-15-2C	310	1.5 mm	Y	Y	Y	Y	N/A
					PEC-15-9	276/80	1 mm		Y	Y	-	-
					PEC-15-27	285	~5mm (partially exposed)	Y	Y	Y	-	Y
					PEC-16-3	285	Exposed	-	Y	-	-	-
VIII	335256.84W 4864727.56N	Veralum/Lower Lindsay	Roadside outcrop	4	-	-	-	-	-	-	-	-
X	320265.00W 4859287.00N	Upper Lindsay	Lake Ontario Shoreline: Salmon Point	122	PEC-15-4	280/76	7 - 9 mm	Y	Y	Y	-	-
					PEC-15-31A	274	2.1 cm	Y	Y	Y	Y	N/A
					PEC-15-31BI	271	>6mm	Y	Y	Y	-	-
					PEC-15-31BIII		vug-filled crystals		Y	Y	-	-
					PEC-15-31C	272	4mm	Y	Y	Y	-	-
XI	294264.44W 4872085.79N	Upper Lindsay	Lake Ontario Shoreline	51	PEC-15-5A	025/57	Exposed	Y	Y	Y	Y	N/A
					PEC-15-5B	255	Exposed	Y	Y	Y	-	-
XIII	333646.11W 4906239.71N	Gull	Roadside outcrop: Desronto Rd	16	PEC-15-6	225/73	1.5 mm	Y	Y	Y	-	-
					PEC-15-7	015/86	2.5 mm	-	Y	Y	-	-
XIV	283259.60W 4874018.90N	Lower Lindsay	Lake Ontario Shoreline: Presqu'ile National Park	13	-	-	-	-	-	-	-	-
XV	283584.80W 4874190.60N	Lower Lindsay		10	-	-	-	-	-	-	-	-
XVI	281163.06W 4874613.40N	Lower Lindsay		10	PEC-15-8	215	1 mm	Y	Y	Y	Y	N/A
XVII	335118.01W 4878231.50N	Lower Lindsay	Forested area	5	-	-	-	-	-	-	-	-
XVIII	337816.43W 4877172.87N	Veralum/Lower Lindsay	Roadside outcrop: Mosquito Ln	38	PEC-15-10	232/86	Exposed	-	Y	Y	-	-
					PEC-15-28	312	Exposed	-	Y	Y	-	-
XIX	330108.00W 4872085.79N	Veralum/Lower Lindsay	Peninsula shoreline: Little Bluff	3	-	-	-	-	-	-	-	-
XX	347366.29W 4878058.74N	Veralum	Peninsula shoreline: County Rd 8	4	PEC-15-11	090/85	Exposed	-	Y	Y	-	-
XXV	332759.00W 4865859.00N	Lower Lindsay	Roadside outcrop: County road 10	15	PEC-15-26	256	1.5 mm	-	Y	Y	-	-
XXVI	326329.00W 4857319.00N	Upper Lindsay	Lake Ontario Shoreline	289	PEC-15-30	242	1.5 mm	Y	Y	Y	Y	N/A
					PEC-16-1	267	8 mm	Y	Y		-	-
					PEC-16-2	250	4 mm	Y	Y		-	-
XXIX	299833.00W 4866725N	Upper Lindsay	Lake Ontario Shoreline: Huick's Point	57	PEC-15-32A	273	1.5 mm		Y	Y	-	-
					PEC-15-32B	273	1.5 mm	Y	Y	Y	-	-
XXXI	298893.00W 4872686.00N	Upper Lindsay	Quarry: *Concecon(Lafarge)*	12	-	-	-	-	-	-	-	-
XXXII	319786.00W 4876486.00N	Lower Lindsay	Quarry: *Foster Rock*	31	PEC-16-4A	087/80	3 mm	Y	Y	-	-	-
					PEC-16-4B	268/72	2.5 mm	Y	Y	-	-	-
					PEC-16-4C	135/74	1.5 cm; quartz vein	Y	-	-	-	-
XXXIII	330646.00W 4881687.00N	Lower Lindsay	Quarry: *Miller Paving Limited*	8	-	-	-	-	-	-	-	-
XXXIV	323918.00W 4885387.00N	Lower Lindsay	Quarry: *Power Concrete Products*	13	-	-	-	-	-	-	-	-
XXXV	324630.00W 4886760.00N	Lower Lindsay	Quarry: Abandoned	26	-	-	-	-	-	-	-	-
XXXVI	311508.00W 4883147.00N	Lower Lindsay	Quarry: *Mountain view*	7	-	-	-	-	-	-	-	-
XXXVII	324399.00W 4859643.00N	Upper Lindsay	Lake Ontario Shoreline	9	-	-	-	-	-	-	-	-
XXXVIII	330108.00W 4858226.00N	Lower Lindsay	Lake Ontario Shoreline	100	-	-	-	-	-	-	-	-
XXXIX	341398.00W 4862767.00N	Lower Lindsay	Lake Ontario Shoreline: Ostrander Rd.	126	PEC-16-5	281	4 mm	Y	Y	-	-	-
XLII	349826.02W 4865640.24N	Veralum	Lake Ontario shoreline; Structures measured via satellite imagery	457	-	-	-	-	-	-	-	-
XLIII	338986.34W 4861710.02N	Lower Lindsay		79	-	-	-	-	-	-	-	-
XLIV	316919.99W 4862357.77N	Upper Lindsay		25	-	-	-	-	-	-	-	-

* All UTM coordinance are in zone 18T; Rock formations are all middle-Ordovician; N/A: Samples awaiting 3He/4He analysis

Table 2: Trace element geochemistry and stable isotope results of calcite veins dated via U-Pb ages or with for $^{3}He/^{4}He$ values

Station	Sample Number	δ13C PDB (‰)	δ18O SMOW (‰)	Ca (Wt%)	Mg (ppm)	Mn (ppm)	Sr (ppm)	Y (ppm)	La (ppm)	Ce (ppm)	Pr (ppm)	Nd (ppm)	Sm (ppm)	Gd (ppm)	Tb (ppm)	Dy (ppm)	Ho (ppm)	Er (ppm)	Tm (ppm)	Yb (ppm)	Lu (ppm)	ΣREE (ppm)	U ±1σ	U/Pb ages ± 1σ (Ma)	$^{3}He/^{4}He$ (R/Ra)	^{4}He ± 1σ (g/cc)
I	PEC-15-13	0.49	19.65	55.17	2309.08	567.37	195.24	0.42	0.04	0.25	0.06	0.37	0.11	0.10	0.01	0.08	0.02	0.04	0.01	0.03	0.00	1.13	-	-	0.42±0.1	3.20E-05
II	PEC-15-25A	5.68	23.65	55.00	625.5	228.91	155.13	3.68	1.95	6.77	1.08	4.74	1.10	1.01	0.13	0.75	0.14	0.36	0.05	0.27	0.04	18.65	17.3 ± 3.8	120±63	-	-
	PEC-15-2A	5.57	22.57	54.30	234.5	1459.52	54.34	0.47	0.07	0.20	0.04	0.21	0.07	0.09	0.01	0.08	0.02	0.05	0.01	0.05	0.01	0.92	80 ± 17	81.4±8.3	-	-
VII	PEC-15-2C	2.88	22.70	54.91	241.11	1885.39	47.96	0.21	0.03	0.13	0.03	0.17	0.05	0.04	0.01	0.04	0.01	0.03	0.00	0.03	0.01	0.59	113 ± 24	87±45	-	-
	PEC-15-27	5.83	22.90	54.77	332.05	909.01	62.12	0.17	0.01	0.04	0.01	0.06	0.02	0.03	0.00	0.02	0.01	0.02	0.00	0.03	0.01	0.25	-	-	2.7±.04	1.90E-06
X	PEC-15-31A	0.12	23.03	55.01	201.03	1377.71	22.03	5.58	32.94	87.82	11.19	47.63	4.77	2.71	0.27	1.30	0.26	0.77	0.13	1.08	0.19	191.79	106.9 ± 5.4	110.4±2.4	-	-
XI	PEC-15-5A	-0.28	19.52	53.82	2740.93	3327.52	188.07	46.39	14.93	64.12	11.77	48.06	10.82	10.13	1.44	7.69	1.43	3.42	0.42	2.24	0.31	178.84	7.6 ± 1.9	Discordant age	-	-
XVI	PEC-15-8	1	24.04	54.07	546.28	8173.94	30.18	229.65	32.59	72.61	9.21	39.92	13.97	27.19	4.95	31.03	7.07	18.87	2.13	9.95	1.47	273.09	131 ± 28	110.7±6.8	-	-
XXVI	PEC-15-30	-0.13	23.67	54.38	6551.54	130.1	333.02	0.78	0.38	0.62	0.08	0.33	0.07	0.09	0.01	0.10	0.02	0.07	0.01	0.05	0.01	1.86	318 ± 68	-164±270	-	-

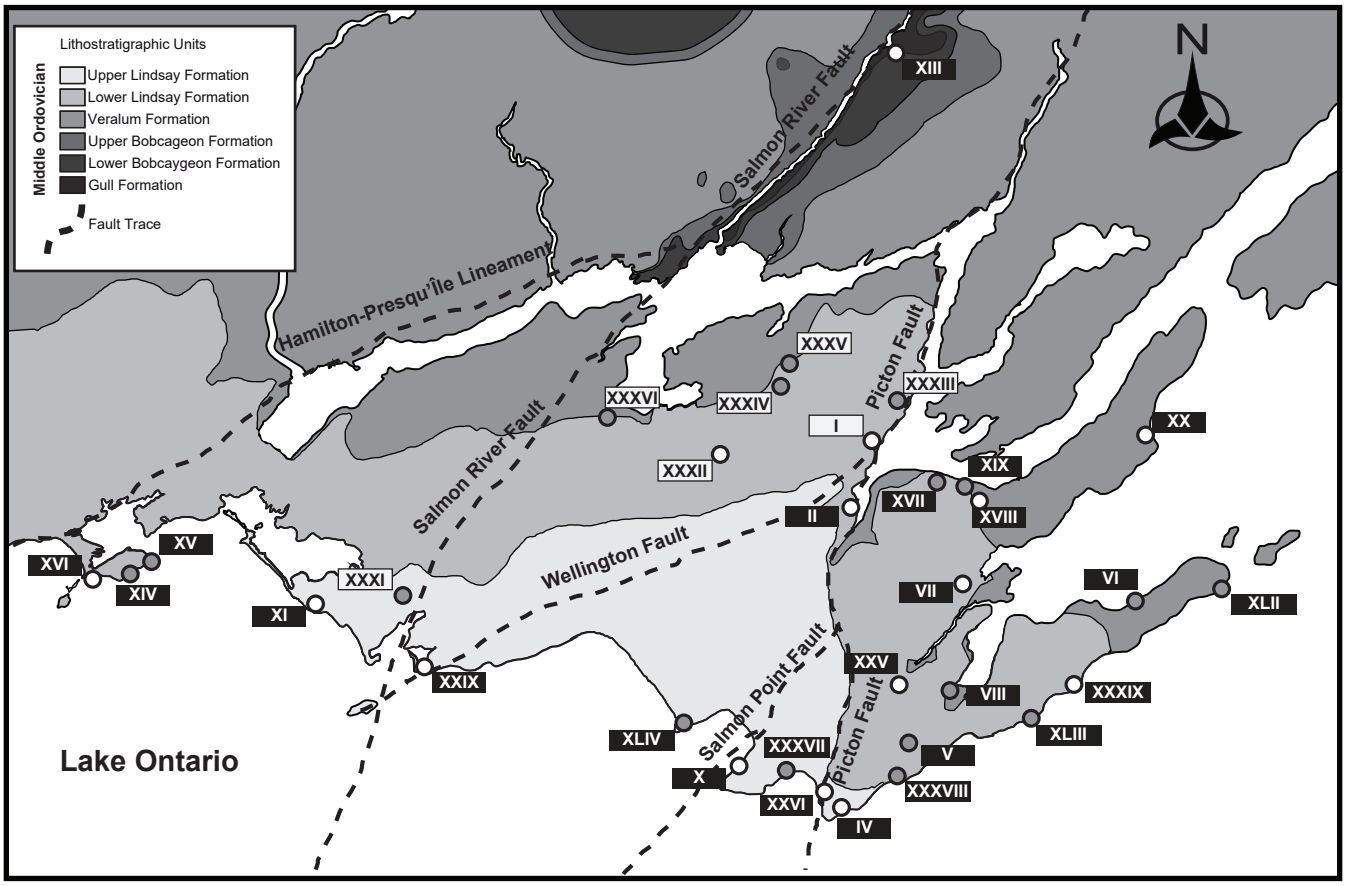

Figure 1 | Simplified geological map of Prince-Edward-County, Southern Ontario. Outcrop distribution of 32 visited stations represented by roman numerals. White dots represent stations where samples were collected, grey dots represent stations where exclusively structural measurements were taken. Numerals with a white backdrop represent quarries. (Geological map of the Paleozoic strata of Prince-Edward-County was created from a compilation of preliminary maps P2412, P2374 and P2375 from the Ontario Geological Survey; D.M Carson, 1981, fault trace positions; McFall, 1993)

Figure 2A

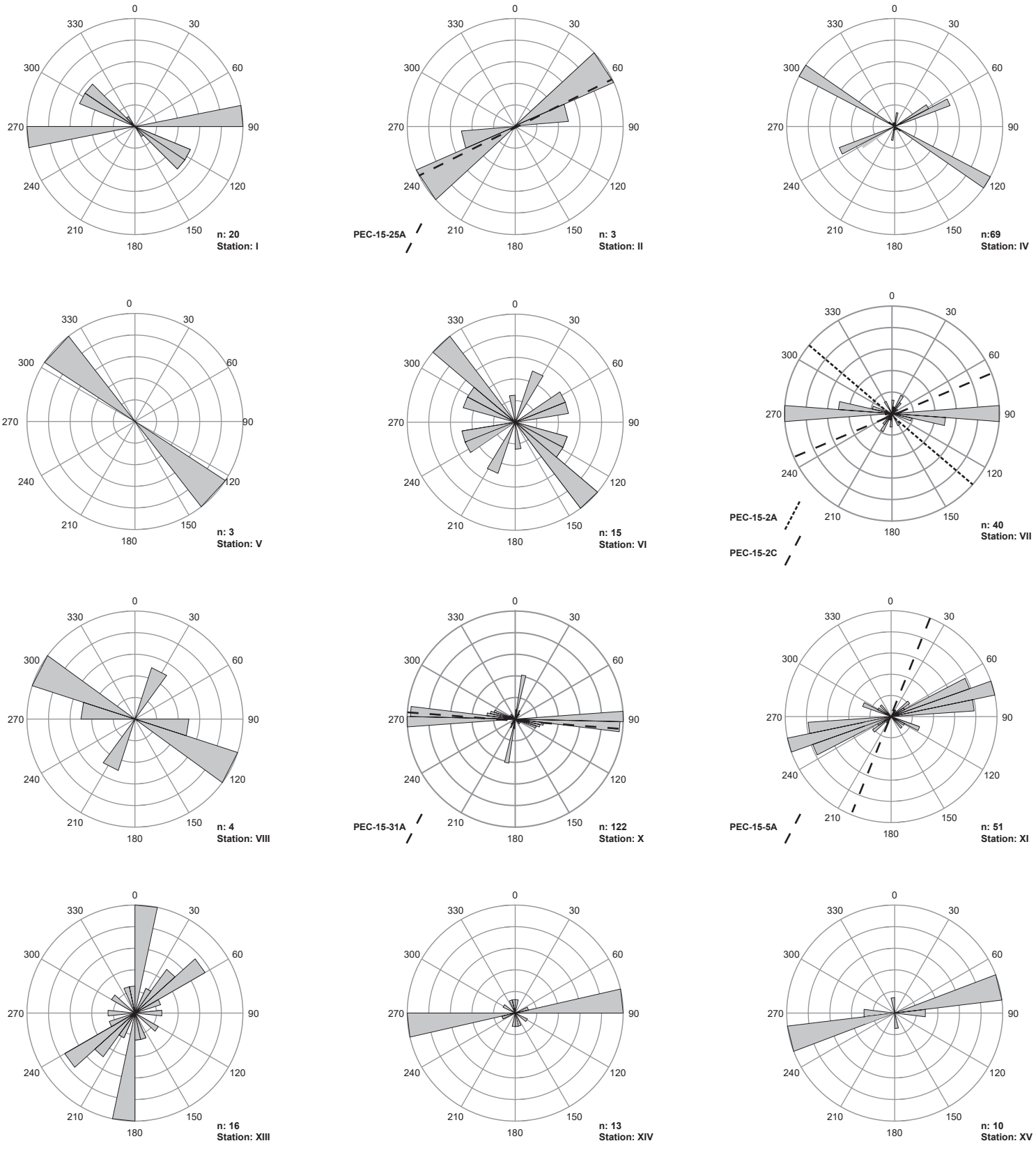
0
30
60
90
120
150
180
210
240
270
300
330
n: 20
Station: I
PEC-15-25A
n: 3
Station: II
n:69
Station: IV
n: 3
Station: V
n: 15
Station: VI
PEC-15-2A
PEC-15-2C
n: 40
Station: VII
PEC-15-31A
n: 122
Station: X
PEC-15-5A
n: 51
Station: XI
n: 4
Station: VIII
n: 16
Station: XIII
n: 13
Station: XIV
n: 10
Station: XV

Figure 2B

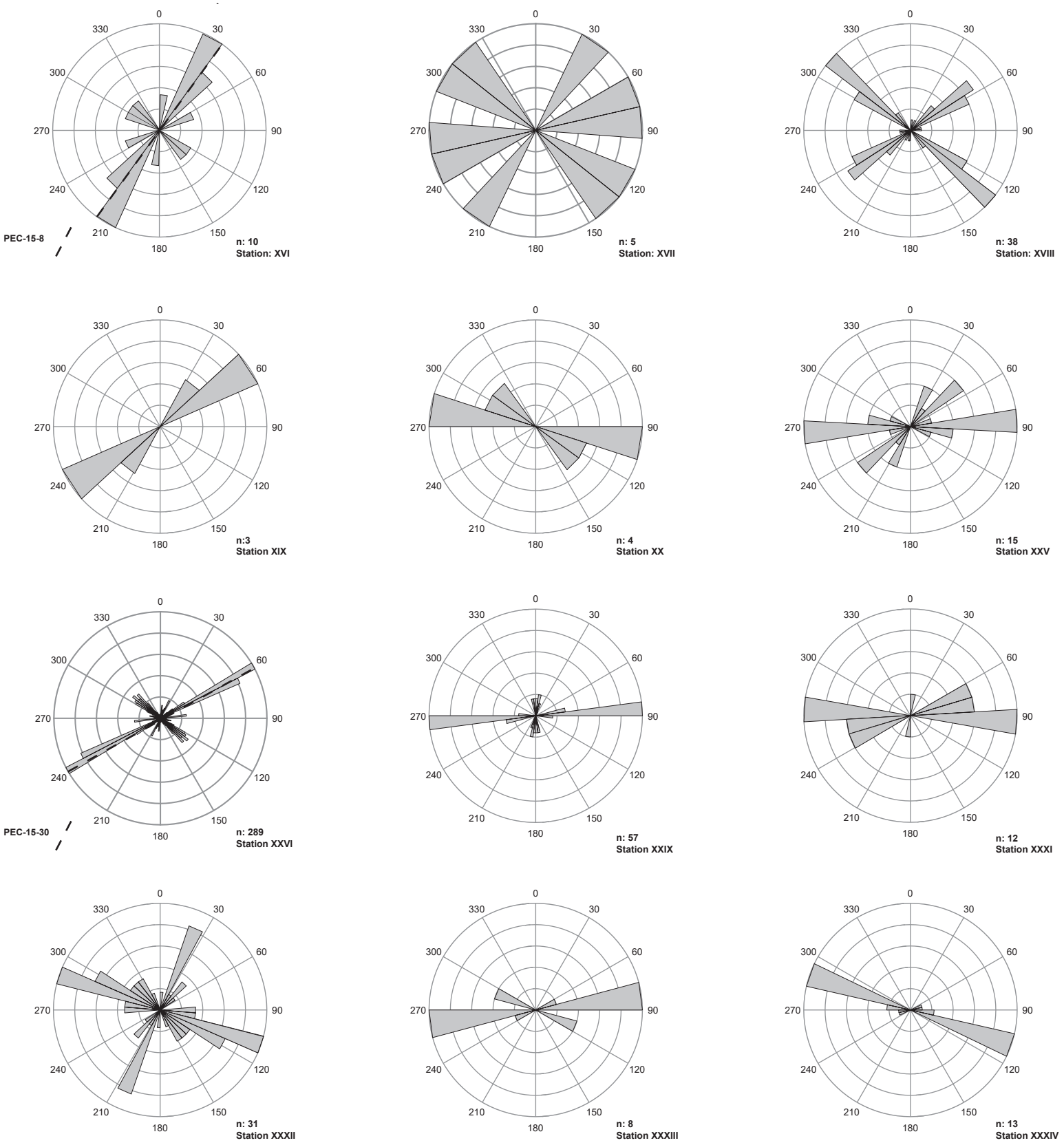
0
30
60
90
120
150
180
210
240
270
300
330
PEC-15-8
n: 10
Station: XVI
n: 5
Station: XVII
n: 38
Station: XVIII
n:3
Station XIX
n: 4
Station XX
n: 15
Station XXV
PEC-15-30
n: 289
Station XXVI
n: 57
Station XXIX
n: 12
Station XXXI
n: 31
Station XXXII
n: 8
Station XXXIII
n: 13
Station XXXIV

Figure 2C

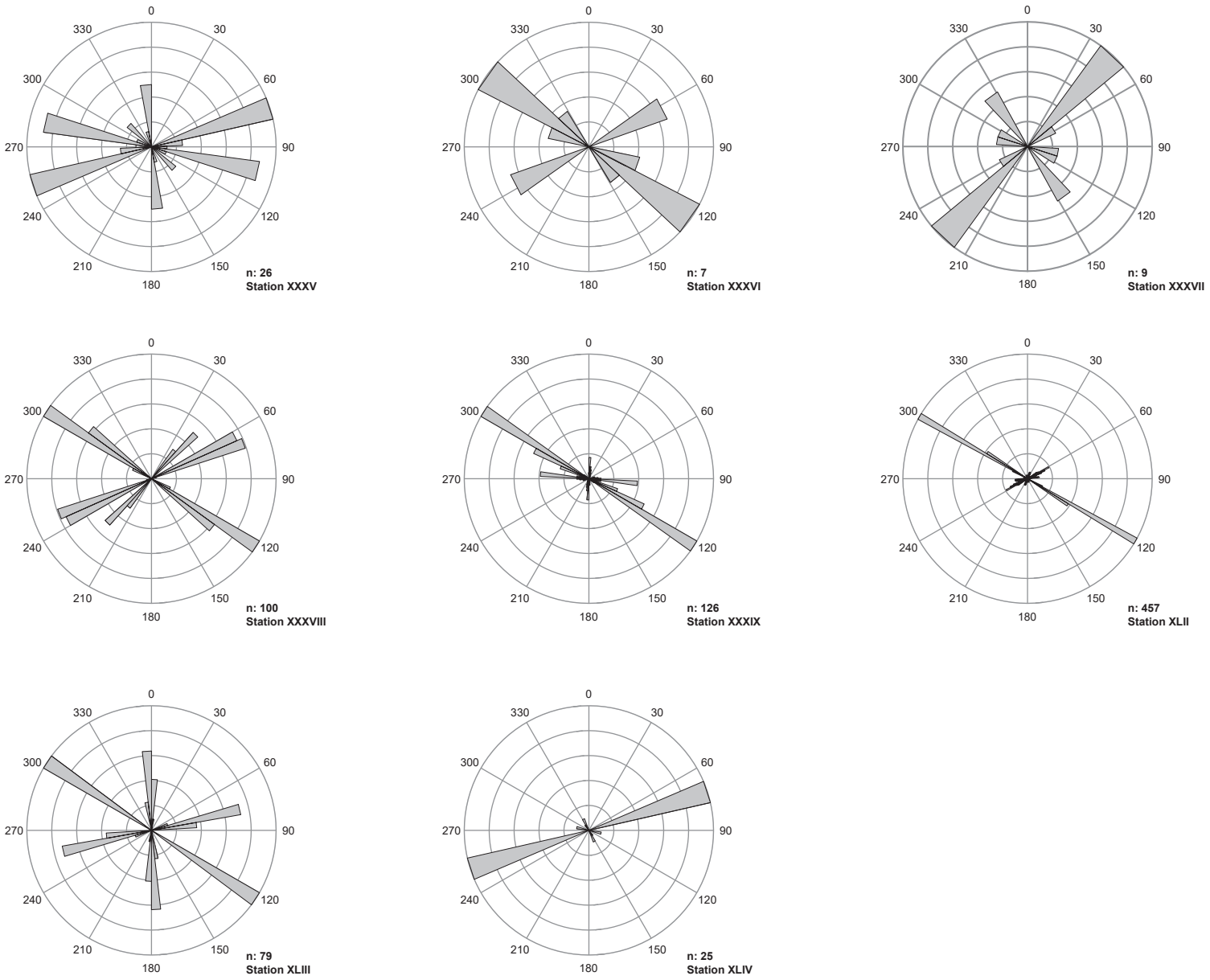

Figure 2 | Rose diagrams projecting the frequency of sub-vertical joints measured from all 32 stations. Roman numerals correspond to stations represented in Figure 1. Calcite veins dated via U-Pb are projected as dashed lines at their respective stations. Two prominent joint populations are identified: trending NW-SE and broadly E-W. Bin-sizes are proportional to the square root of the total number of joint measurements (n), a complete description is available in the methods section of the report

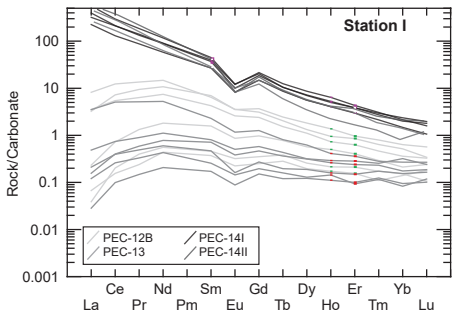

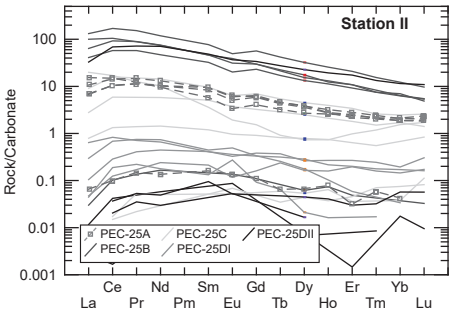

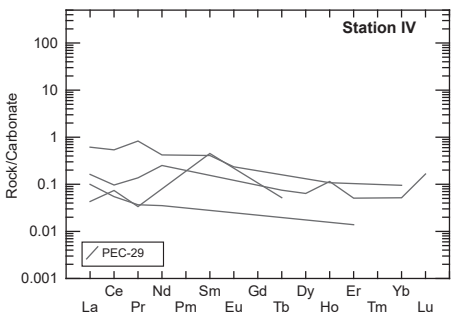

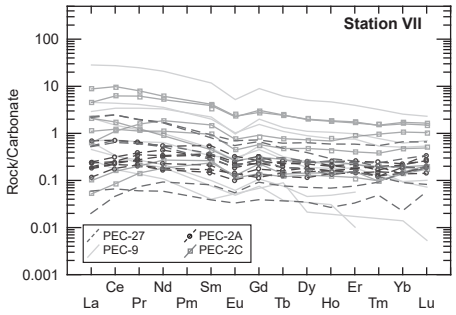

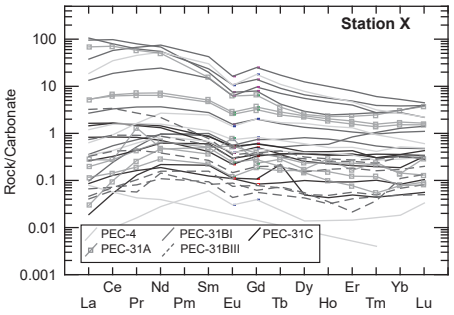

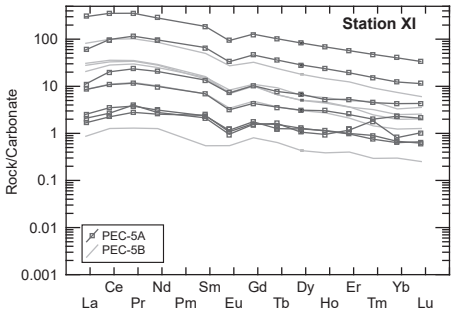

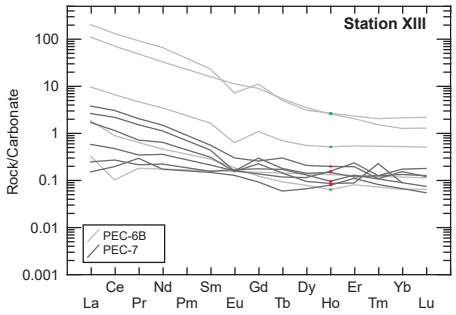

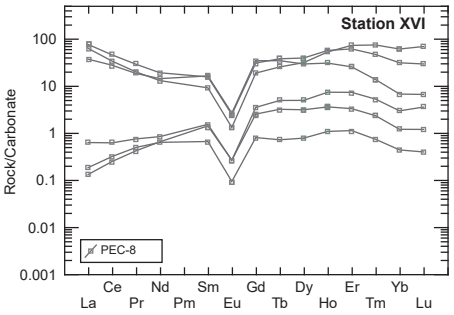

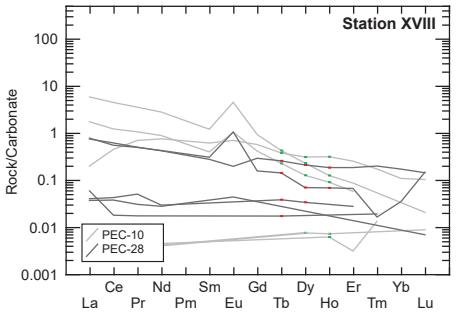

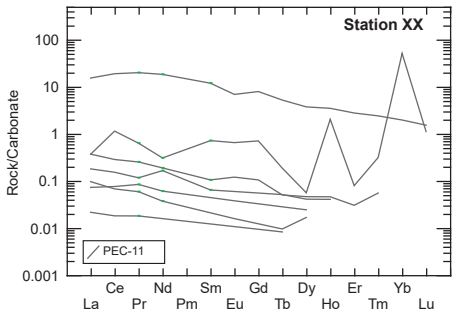

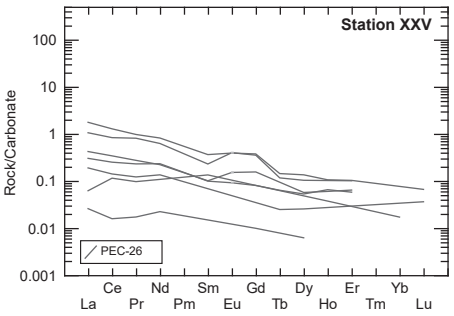

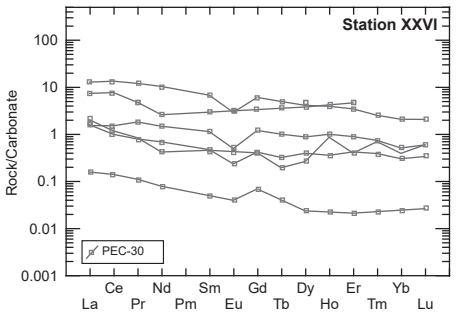

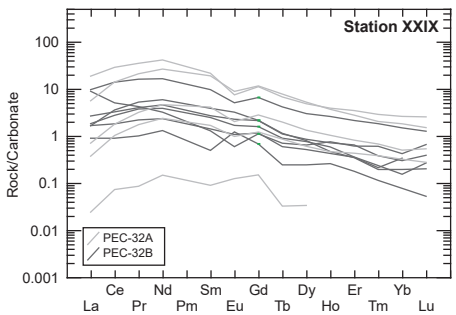

Figure 3 | Spider plots of calcite veins measured via LA-ICP-MS. Each plot represents a station, identified by roman numerals corresponding to the locations illustrated in Figure 1. Stations where multiple samples were collected are differentiated by different increments of grey. Each line corresponds to a point analysis; three to seven measurements were taken on each sample. Calcite veins dated via U-Pb are represented by symbols. Samples with an enriched δ13C signature (refer to figure 4) are represented by dashed lines. All samples were collected in 2015, and the "15" has been removed from sample numbers

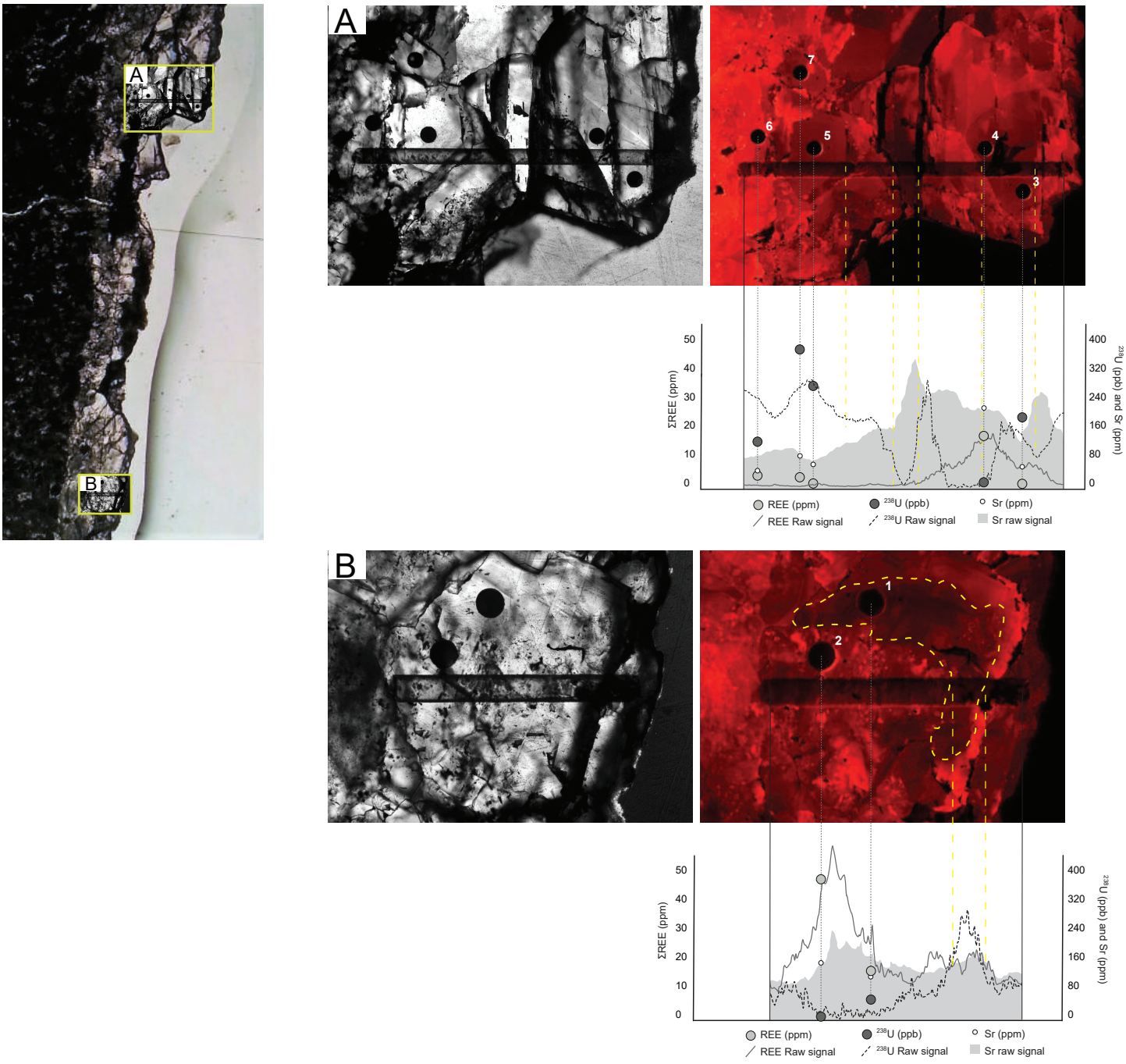

Figure 4 | LA-ICP-MS traverse profiles and point analysis for REE's, ^{238}U and Sr. Relative position of traverses A and B are highlighted by yellow boxes in thick-section photo (left). Photomicrographs of the ablated traverses in cathodoluminescence are aligned with the raw signal acquired, projected in the diagrams below: Black vertical lines mark the start/end of the traverse and vertical yellow-dashed lines mark crystal boundaries. Measurements from point-analysis are projected as points in the diagram: REE's are measured in ppm, corresponding to the vertical axis on the left, ^{238}U is measured in ppb and Sr is measured in ppm corresponding to the vertical axis on the right. Calcite crystals vary in composition. Traverse A shows ^{238}U residing at crystal boundaries and the relative abundance of REE's varying in different crystals. Traverse B shows REE's residing in crystal domains with abundant fluid inclusions (refer to photomicrograph in PPL), and ^{238}U residing at crystal boundaries as well as in crystal domains that are quenched under CL (white dashed line). REE and ^{238}U distribution seem to be inversely correlated. The numbered points are the names of the spot analysis listed in appendix D where geochemical values are available. Ablation pits from point analysis are 100 µm in diameter for scale

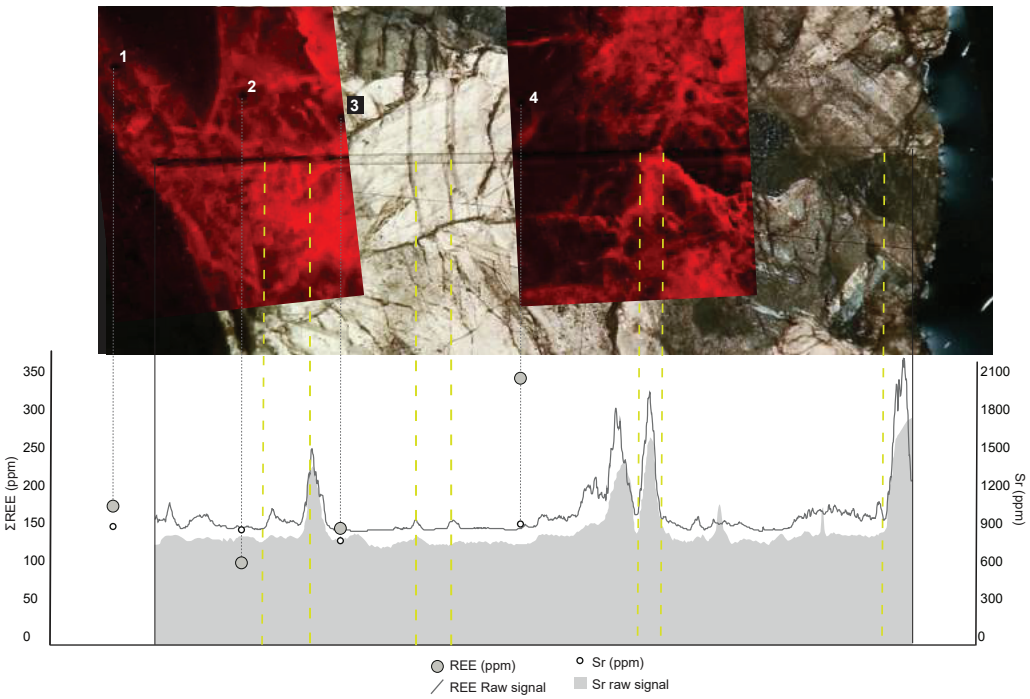

Figure 5 | LA-ICP-MS traverse profile and point analysis for REE's and Sr. The ^{238}U signal from the traverse is flat, and exluded from this figure. A compilation of photomicrograph of the ablated traverses in cathodoluminescence and CPL are aligned with the raw signal acquired, projected in the diagram below: Black vertical lines mark the start/end of the traverse and vertical yellow-dashed lines mark crystal boundaries. Measurements from point-analysis are projected as points in the diagram. REE's and Sr are measured in ppm, REE values correspond to the vertical axis on the left, and Sr values correspond to vertical axis on the right. Calcite crystal appear to be relatively homogenous in composition, and are enriched in Sr (>600 ppm). Peaks in the REE signal align with crystal boundaries that are ignite under CL, and fractures in calcite crystals. The numbered points are the names of the spot analysis listed in appendix D where geochemical values are available. Ablation pits from point analysis are 100 µm in diameter for scale

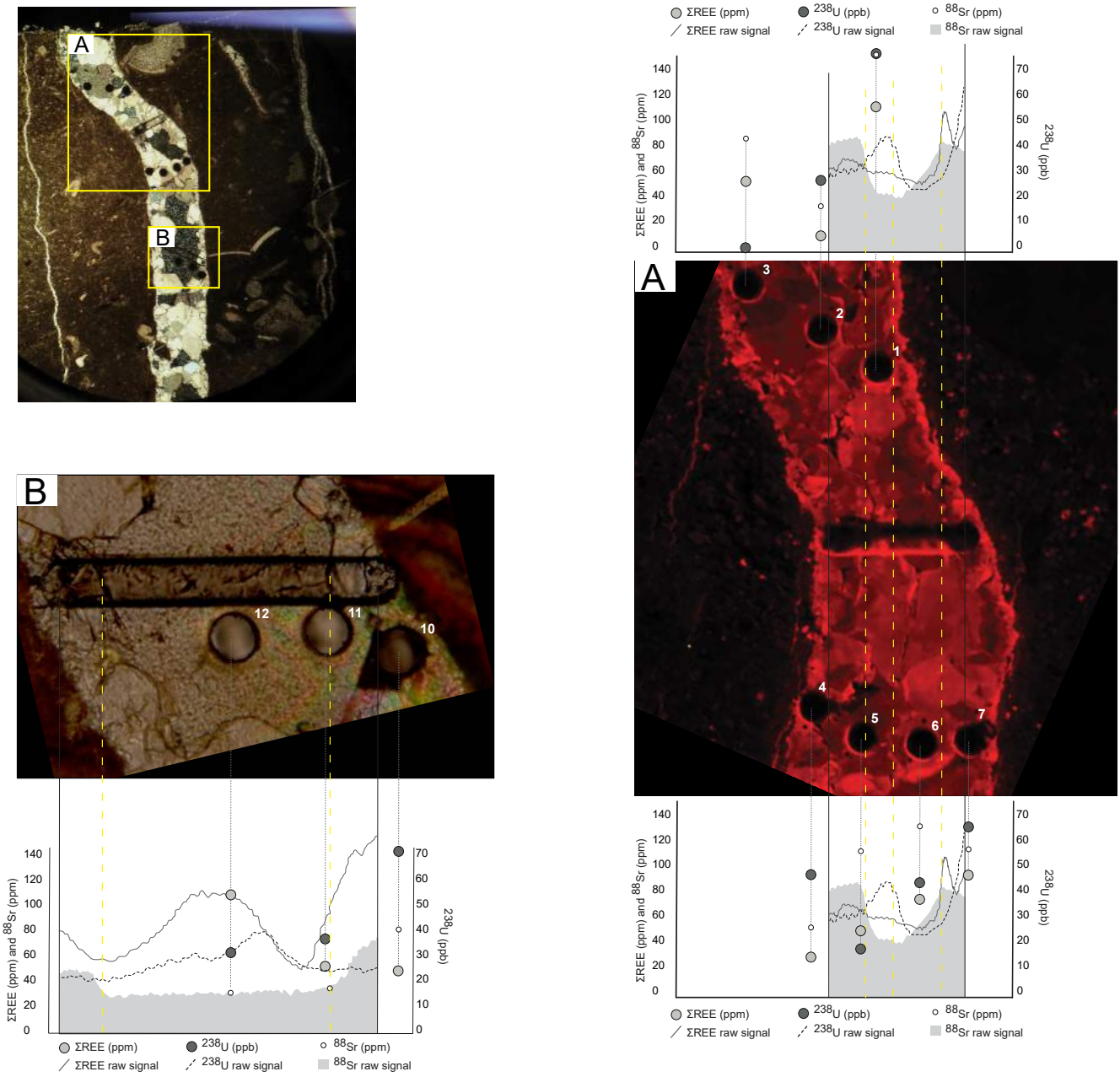

Figure 6 | LA-ICP-MS traverse profiles and point analysis for REE's, ^{238}U and Sr. Relative position of traverses A and B are highlighted by yellow boxes in thick-section photo. Photomicrographs of the ablated traverses in PPL/CL aligned with the raw signal acquired, projected on their respective diagrams. Black vertical lines mark the start/end of the traverse and yellow-dashed lines mark crystal boundaries. Measurements from point-analysis are projected as points in the diagram: REE's and Sr are measured in ppm, and correspond to the vertical axis on the left. ^{238}U is measured in ppb and corresponds to the vertical axis on the right. Calcite crystal vary in composition. All traverses signals suggest theres an enrichment in Sr in small crystals residing at the vein-wall-rock interface. The large equant crystal in the center of traverse B is zoned in ^{238}U and REE's. In traverse B, ^{238}U and REE's are concentrated at crystal boundaries. The numbered points are the names of the spot analysis listed in appendix D where geochemical values are available. Ablation pits from point analysis are 100 µm in diameter for scale

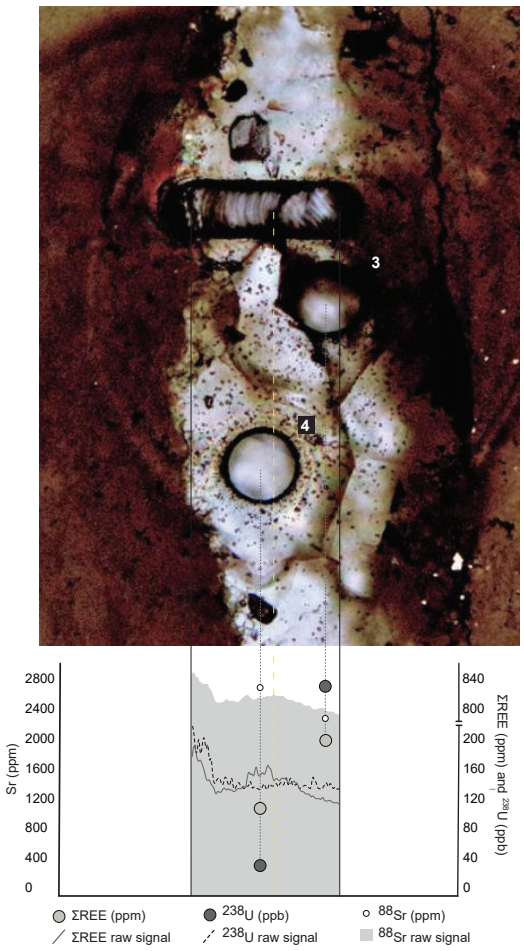

Figure 7 | LA-ICP-MS traverse profiles and point analysis for REE's , ^{238}U and Sr . Photomicrograph of the ablated traverses in PPLc is aligned with the raw signal acquired, projected in the diagrams below: Black vertical lines mark the start/end of the traverse and vertical yellow-dashed line mark crystal boundaries. Measurements from point-analysis are projected as points in the diagram: Sr is measured in ppm, corresponding to the vertical axis on the left, ^{238}U is measured in ppb and Sr is measured in ppm corresponding to the vertical axis on the right. Calcite vein is relatively enriched in Sr (>1600 ppm). Calcite crystals have fluid inclusions. Point 3 is located at a crystal boundary and is enriched in ^{238}U and REE's. The numbered points are the names of the spot analysis listed in appendix D where geochemical values are available. Ablation pits from point analysis are 100 µm in diameter for scale

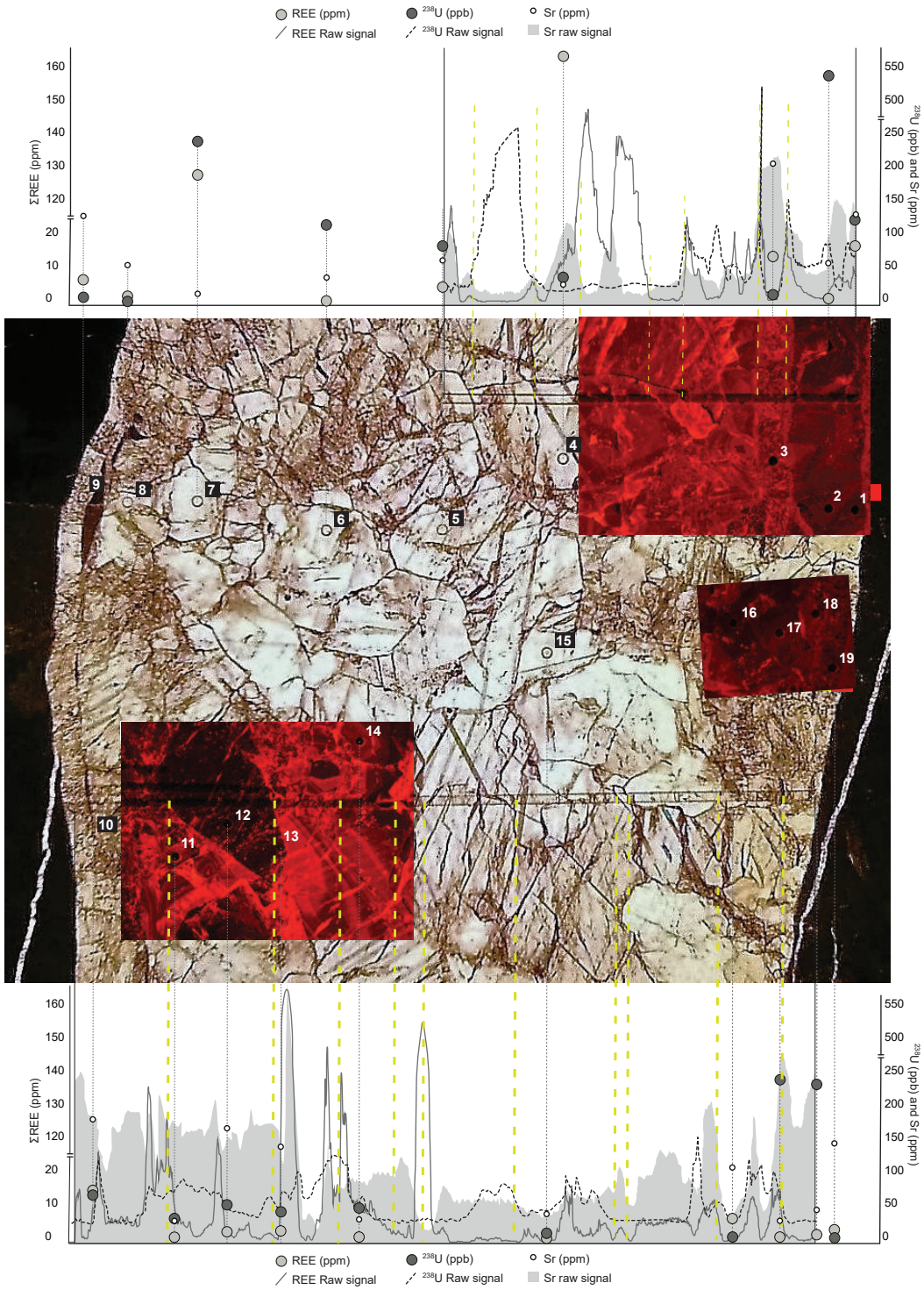

Figure 8 | LA-ICP-MS traverse profiles and point analysis for REE's , ^{238}U and Sr. Photomicrographs of the ablated traverses in cathodoluminescence are aligned with the raw signal acquired, projected in the diagrams above and below: Black vertical lines mark the start/end of the traverse and vertical yellow-dashed lines mark crystal boundaries. Measurements from point-analysis are projected as points in the diagram: REE's are measured in ppm, corresponding to the vertical axis on the left, ^{238}U is measured in ppb and Sr is measured in ppm corresponding to the vertical axis on the right. Calcite crystals vary in composition. Sr concentrations vary in different crystals. ^{238}U and REE peaks allign with opaque material residing at recrystalized grain boundary. The numbered points are the names of the spot analysis listed in appendix D where geochemical values are available. Ablation pits from point analysis are 100 µm in diameter for scale

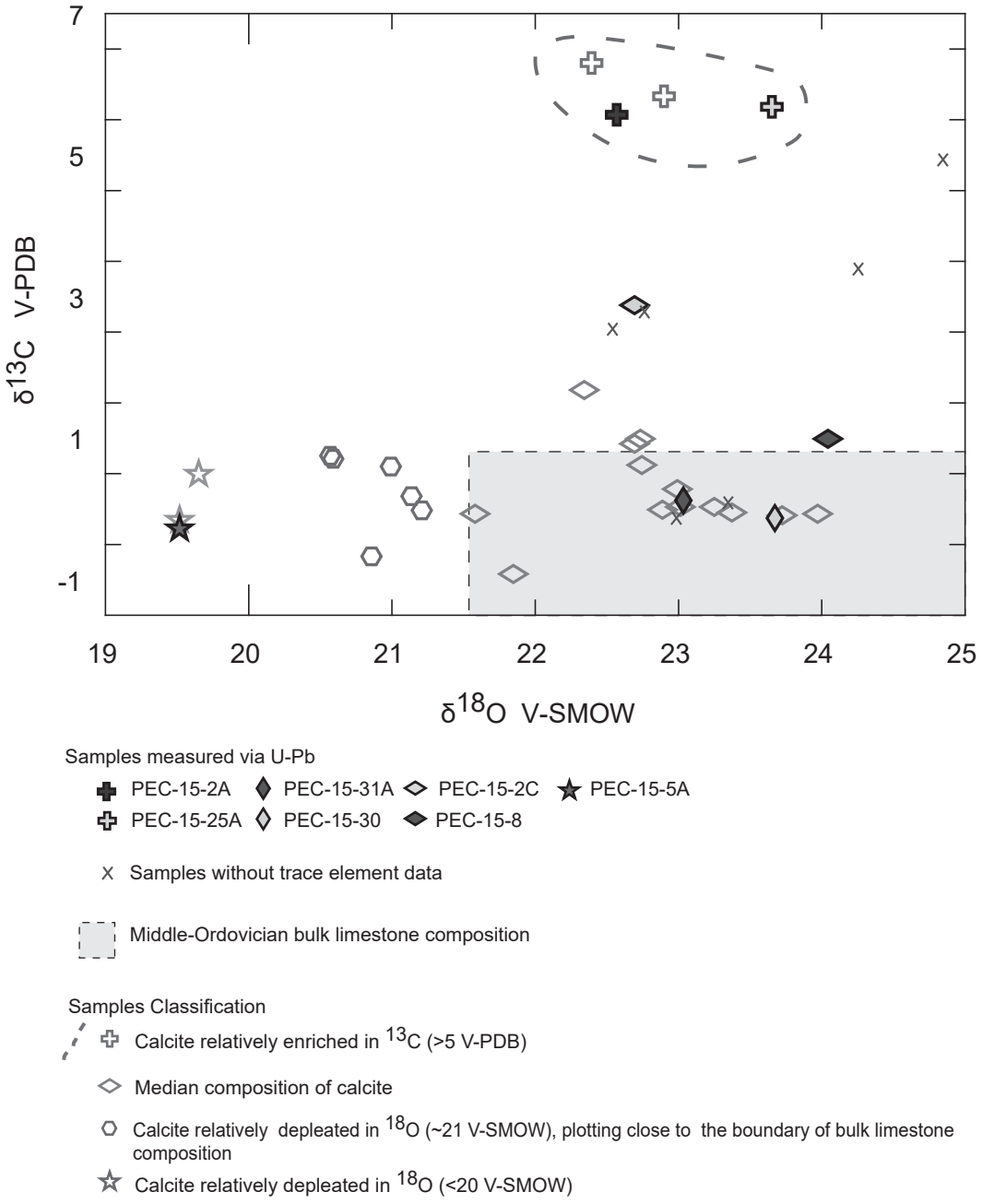

Figure 9 | Carbon vs. oxygen isotopic composition of 36 calcite veins. Samples measured via U-Pb are distinguished by their respected symbols, and samples without trace element geochemistry are represented by an “x” symbol. Other samples are grouped based on their isotopic signature. Samples with an enriched δ13C signature are contoured by a dashed line and are also distinguished by dashed lines in their respective spider plots in figure 3. (Middle-Ordovician bulk limestone composition is from Coniglio et al. 1994.)

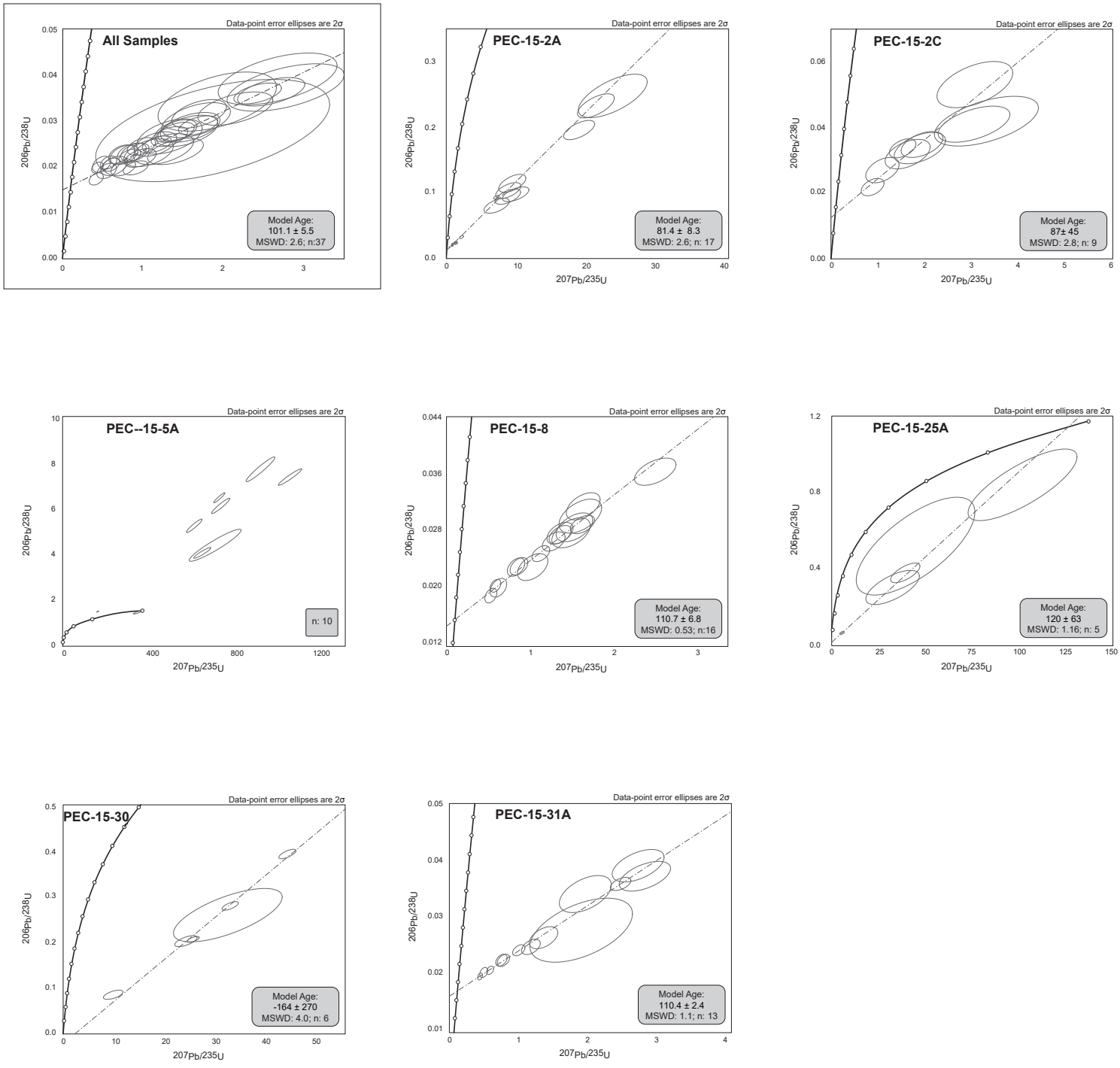

Figure 10 | U-Pb concordia diagrams measured via LA-ICP-MS yielding model ages of calcite mineralizing. Diagrams of seven samples that were dated, as well as a compilation of all measurements regressed on a single concordia diagram (contoured by black box). (n = number of measurements)